Origin of the Pairing Interaction in the Theory of Superconductivity*

Leon N Cooper
Brown University, Providence, Rhode Island 02912

and

Birger Stölan
Norwegian Institute of Technology, University of Trondheim, Trondheim, Norway
(Received 18 January 1971)

A strongly coupled many-body system (a system of fermions confined in a shell surrounding the Fermi surface for which the variation in the single-particle kinetic energy is neglected) is defined. Some general properties of this system are obtained, in particular a criterion for permissible approximations. It is shown that a set of diagrams in which an electron of momentum $-\vec{k}$ and of spin $\downarrow$ interacts with many electrons of momentum $\vec{k}+\vec{q}$ and spin $\uparrow$, where $\vec{q}$ does not grow too large, can be consistently extracted from the totality of graphs generated by this strongly coupled Hamiltonian. When analyzed, these lead to a ground-state and single-particle spectrum displaying the important qualitative features of a BCS superconductor.

I. INTRODUCTION

The phenomenon of superconductivity, generally believed to be due to the instability of the normal Fermi sea under the formation of singlet-spin electron pairs, is described theoretically in various approximations which retain only interactions between electrons of opposite spin and momentum. These $-\vec{k}\downarrow$, $\vec{k}\uparrow$ interactions represent but a small part of the Hamiltonian, and the reason they dominate the behavior of the system—why, for example, the interaction between $-\vec{k}\downarrow$ and $\vec{k}+\vec{q}\uparrow$ (where $\vec{q}$ is small) would not be as important—has never been completely clarified. In this paper we consider the problem of a system of fermions confined in a container, subject to a weak attractive interaction, and attempt, beginning with the full two-body Hamiltonian, to extract in a systematic way from the totality of graphs a subset which can be shown to dominate in the limit that certain parameters become small. This set of diagrams in which an electron of momentum $-\vec{k}$ and spin $\downarrow$ interacts with many electrons of momentum $\vec{k}+\vec{q}$ spin $\uparrow$ (where $\vec{q}$ is not too large) can be analyzed in a consistent manner and results in a single-particle spectrum characteristic of a superconductor. A possible criterion for the validity of the pairing approximation is that these relevant parameters in fact can be small.

The qualitative changes in the "normal" electron wave function, associated with the transition into the superconducting state, seem to be related to the extreme degeneracy of the electron levels at the Fermi surface. Everything indicates a large change for those states near the Fermi surface, but there is no indication at all (in fact the contrary) of anything drastic happening for the others. It appears likely that as the coupling constant goes to zero, the single-particle states involved in the construction of the coherent superconducting state become more and more closely limited to the region surrounding the Fermi surface.

We therefore are led to divide the many-body system into three regions: a region deep inside the Fermi sea (I), a region far outside the Fermi sea (II), and finally the region of interaction just surrounding the Fermi surface. We regard the region of interaction as critical, where the single-particle states are highly degenerate and where the instabilities associated with the appearance of superconducting or superfluid states manifest themselves. We assume that such a region can be defined in the limit of a very weak interaction and that once treated correctly the effects of regions I and II can be taken into account by some perturbative technique.

To simplify matters as much as possible and to focus our attention on what we believe are the relevant points, we replace the kinetic-energy operator in the interaction region by its expectation value

$$T = \langle T \rangle$$

and set this expectation value equal to zero by a shift in the energy scale. This defines what we call a strongly coupled model. It is motivated by the belief that, since the important single-particle states are confined to a small shell around the Fermi surface where the variation in kinetic energy is not large, all of the qualitative results must be contained in this simplified system. A similar strong-coupling approximation to the BCS Hamiltonian yields results that are qualitatively and quantitatively almost the same as those obtained including the variation in kinetic energy.

In addition we include only interactions between electrons of opposite spin (reflecting the fact that for short-range interactions, electrons in a sym-

metric-space state interact more strongly than those in an antisymmetric-space state) and further let the interaction be a constant over the shell of interaction. These simplify, but are not entirely necessary for, what follows. We thus arrive at a completely degenerate, interacting, finite, many-fermion system of $4N$ single-particle levels of both spins to be occupied by $2N$ fermions, half of spin up, the other half of spin down.

In Sec. II the general properties of such a system are reviewed and some comments made on possible criteria for the validity of approximations in many-fermion systems. In order to make this paper reasonably self-contained, we have repeated some earlier results.

In Sec. III an analysis of the graphs generated by the strongly coupled system leads to the definition of what we call the generalized BCS Hamiltonian—a generalization of graphs of the BCS topology (in which an electron of momentum $-\vec{k}$ and spin $\downarrow$ can interact with many electrons in the region surrounding $\vec{k}\uparrow$) and an approximation to the full Hamiltonian which is consistent with the criteria outlined in Sec. II. The weight of these GBCS graphs is then analyzed by a cycle-polygon method.

In Sec. IV the analytic and graphical properties of the strongly coupled BCS Hamiltonian are discussed.

In Sec. V the ground state and excited states of the GBCS Hamiltonian are obtained. The spectrum displays the energy gaps and degeneracies characteristic of the single-particle spectrum of a superconductor.

These results are discussed in Sec. VI, and in the Appendices we display some details of our methods for counting and weighing graphs.

II. STRONGLY COUPLED SYSTEM

A. Definition

The Hamiltonian for a system of fermions interacting via two-body forces may be written

$$H = H_0 + H_1 , \tag{2.1}$$

where

$$H_0 = \sum_\alpha \int d\vec{r}\, \psi_\alpha^*(\vec{r})(-\hbar^2\nabla^2/2m)\psi_\alpha(\vec{r}) , \tag{2.2}$$

$$H_1 = \tfrac{1}{2}\sum_{\alpha,\beta}\int\int d\vec{r}_1 d\vec{r}_2\, \psi_\alpha^*(\vec{r}_1)\psi_\beta^*(\vec{r}_2) \times v(\vec{r}_1-\vec{r}_2)\psi_\beta(\vec{r}_2)\psi_\alpha(\vec{r}_1) , \tag{2.3}$$

where * means adjoint in the second quantized space. For a nonrelativistic fermion system, ψ is a two-component spinor which satisfies the anti-commutation relations

$$\{\psi_\alpha(\vec{r}), \psi_\beta(\vec{r}')\} = 0 ,$$
$$\{\psi_\alpha(\vec{r}), \psi_\beta^*(\vec{r}')\} = \delta_{\alpha\beta}\delta(\vec{r}-\vec{r}') . \tag{2.4}$$

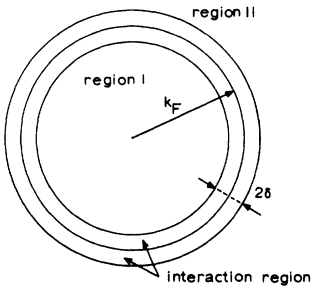

FIG. 1. Interaction shell.

When $v(\vec{r}_1-\vec{r}_2)$ is small enough, only single-particle states in the region immediately surrounding the Fermi surface are greatly altered. We attempt to treat the region of the Hilbert space spanned by these single-particle states with great care assuming that alterations over the rest of the space can be treated as perturbations. To do this we consider the effect of the interaction in the shell surrounding the Fermi surface (the interaction shell) and omit its effect in the inner and outer regions (I and II of Fig. 1).

As $v(\vec{r}_1-\vec{r}_2)$ grows small, the thickness of the interaction shell (and thus the kinetic-energy variation of the single-particle states over this shell) also grows small. We can imagine a limit in which the variation of the kinetic energy over the interaction shell can be neglected entirely and H_0 is replaced by its expectation value $\langle H_0\rangle = T$, the constant average kinetic energy of the system. This defines the strongly coupled system.[1]

In order that such a system have a finite ground-state energy, it would be necessary to limit the region of interaction to some finite domain in momentum space, to provide the cutoff usually provided by the energy denominators. Limiting the interaction to a shell surrounding the Fermi surface preserves the symmetry between particles and holes and is particularly germane since, if the strong-coupling approximation is to make sense, the single-particle states involved must not vary widely in kinetic energy.

These conditions are most conveniently formulated in momentum space. Expanding $\psi_\alpha(\vec{r})$,

$$\psi_\alpha(\vec{r}) = \frac{1}{\sqrt{\Omega}}\sum_{\vec{k},\sigma} c_{\vec{k},\sigma}\, u_\sigma^\alpha\, e^{i\vec{k}\cdot\vec{r}} , \tag{2.5}$$

where Ω is the volume of the system and u_σ^α is a two-component spinor, we obtain [for a spin-independent $v(\vec{r}_1-\vec{r}_2)$]

$$H_1 = \frac{1}{2}\sum_{\substack{\vec{k},\vec{k}',\vec{q},\sigma,\sigma' \\ \vec{k},\vec{k}',\vec{k}+\vec{q},\vec{k}'-\vec{q}\ \text{in shell}}} v(\vec{q})\, c_{\vec{k}+\vec{q},\sigma}^*\, c_{\vec{k}'-\vec{q},\sigma'}^*\, c_{\vec{k}',\sigma'}\, c_{\vec{k},\sigma} , \tag{2.6}$$

where

$$v(\vec{q}) = (1/\Omega)\int v(\vec{r})\, e^{-i\vec{q}\cdot\vec{r}}\, d\vec{r} ,$$

and where we assume that $v(\vec{r})$ is bounded. The anticommutation relations for the c operators are

$$\{c_{\vec{k},\sigma}, c_{\vec{k}',\sigma'}\}=0, \quad \{c_{\vec{k},\sigma}, c^{*}_{\vec{k}',\sigma'}\}=\delta_{\vec{k},\vec{k}'}\delta_{\sigma,\sigma'} . \tag{2.7}$$

We will simplify the notation by setting the constant T equal to zero, thus shifting all energies by T. By the notation $\vec{k}$, $\vec{k}'$, $\vec{k}+\vec{q}$, $\vec{k}'-\vec{q}$ in shell, we mean that the magnitudes of the vectors $\vec{k}$ and $\vec{k}'$ satisfy the condition

$$k_F-\delta<|\vec{k}|<k_F+\delta , \tag{2.8}$$

where presumably $\delta/k_F \ll 1$, while the vector $\vec{q}$ ranges over all values such that $\vec{k}+\vec{q}$ and $\vec{k}'-\vec{q}$ also satisfy (2.8). This has the effect of allowing only those scattering processes which take a particle or hole in the shell defined above into another particle or hole in this shell.

For short-range forces the interaction between antiparallel spins dominates that between parallel spins for which the exchange term is of opposite sign to the direct term. If we thus restrict ourselves to singlet spin states the interaction Hamiltonian becomes

$$H_1=\sum_{\vec{k},\vec{k}',\vec{q}} v(\vec{q})\, c^{*}_{\vec{k}+\vec{q},\uparrow}\, c^{*}_{\vec{k}'-\vec{q},\downarrow} c_{\vec{k}',\downarrow} c_{\vec{k},\uparrow} . \tag{2.9}$$

We assume that the total number of single-particle "unperturbed" states of both spins in the shell defined by (2.8) is $4N$ and that the Fermi surface is symmetrically placed so that the total number of particles is $2N$. Of course, N is proportional to Ω for constant δ. The vacuum state $|\phi_0\rangle$ of the unperturbed system is defined so that all single-particle levels below k_F are filled, while all single-particle levels above k_F are empty. All other "unperturbed" configurations $|\phi_i\rangle$ (there are a total of $\{(2N)!/[(N)!]^2\}^2$ configurations) can be obtained by creating holes below and particles above the Fermi surface, keeping N constant. These are constructed from the vacuum by operating on it with the creation operators $c^{*}_{\vec{k},\sigma}$, $c_{\vec{l},\sigma}$ where $\vec{k}$ lies above the Fermi surface and $\vec{l}$ lies below:

$$|\phi_{\vec{k}_1\cdots\vec{k}_s;\,\vec{l}_1\cdots\vec{l}_s}\rangle = c^{*}_{\vec{k}_1}\cdots c^{*}_{\vec{k}_s}\, c_{\vec{l}_1}\cdots c_{\vec{l}_s}|\phi_0\rangle . \tag{2.10}$$

Creation and annihilation operators can be defined, as has been pointed out by Hugenholtz and Van Hove[2] for arbitrary definitions of the vacuum states. One can consider as the vacuum state any of the unperturbed states of the system, referring all other states to this vacuum by the addition of particles or holes. With respect to this arbitrarily defined vacuum, $c^{*}_{\vec{k}}$ is a creation operator if $\vec{k}$ is one of the states unoccupied in the vacuum, and it is an annihilation operator if $\vec{k}$ is one of the states occupied in the vacuum. On the other hand, $c_{\vec{k}}$ is considered a creation operator if $\vec{k}$ is one of the states occupied in the vacuum. Any results obtained for vacuum expectation values of operators not depending explicitly upon a particular choice of the vacuum state are equally valid for any diagonal matrix elements with all quantities suitably redefined. We will have explicit examples of such behavior later.

As far as the strongly coupled theory is concerned any "unperturbed" state of momentum zero (since it has zero kinetic energy) is as good a vacuum as the $|\phi_0\rangle$ we choose. However, as a state which is related to the vacuum of the full theory, $|\phi_0\rangle$ is preferred since in the full theory $|\phi_0\rangle$, as defined above, has the lowest kinetic energy.

In the limit that $v(\vec{q})$ does not vary over the interaction shell, we set

$$v(\vec{q})=g \tag{2.11}$$

and obtain

$$H_1=g\sum_{\vec{k},\vec{k}',\vec{q}} c^{*}_{\vec{k}+\vec{q},\uparrow}\, c^{*}_{\vec{k}'-\vec{q},\downarrow} c_{\vec{k}',\downarrow} c_{\vec{k},\uparrow} . \tag{2.12}$$

The BCS interaction Hamiltonian

$$H_{BCS}=-V\sum_{\vec{k},\vec{k}'} c^{*}_{\vec{k}',\uparrow}\, c^{*}_{-\vec{k}',\downarrow} c_{-\vec{k},\downarrow} c_{\vec{k},\uparrow} \tag{2.13}$$

is extracted from (2.12) by retaining only interactions between electron pairs of opposite momentum and by setting

$$g=-V , \tag{2.14}$$

where

$$V=|V| .$$

The strongly coupled model of a superconductor (2.13) has previously been discussed by, among others, Anderson[3] and Thouless[4] using nonperturbational methods. The full strongly coupled system (2.12) has also been studied by the present authors[5,6]; in the rest of Sec. II we briefly review some of our previous results which are relevant.

B. Expansion in Coupling Constant

To analyze the strongly coupled system we make use of the resolvent operator $R(z)$ defined by

$$R(z)=1/(H-z) . \tag{2.15}$$

This operator has been discussed previously in connection with the many-body problem by Hugenholtz[7] and Van Hove.[8] If we expand the vacuum state of the unperturbed system $|\phi_0\rangle$ in the eigenfunctions $|\psi_m\rangle$ of the interaction Hamiltonian H_1, where

$$H_1|\psi_m\rangle=E_m|\psi_m\rangle , \tag{2.16}$$

and so that

$$|\phi_0\rangle=\textstyle\sum_m |\psi_m\rangle\langle\psi_m|\phi_0\rangle , \tag{2.17}$$

the vacuum expectation value of the resolvent operator is

$$\langle R(z)\rangle_0 \equiv \langle\phi_0|R(z)|\phi_0\rangle = \sum_m |\langle\phi_0|\psi_m\rangle|^2 (E_m - z)^{-1}. \tag{2.18}$$

The analytic properties of $\langle R(z)\rangle_0$ are immediately evident from this last expression, since the sum is finite. The matrix elements of the resolvent operator are analytic everywhere except for poles on the real axis, and these poles are bounded both above and below by the maximum and minimum energy levels $E_0 < E < E_{max}$. Such maximum and minimum energies exist, since the strongly coupled system is *finite* and $v(\vec{r})$ is bounded.

To evaluate $\langle\phi_0|R(z)|\phi_0\rangle$ we make an expansion in powers of the coupling constant g in H_1,

$$\langle\phi_0|R(z)|\phi_0\rangle = -\frac{1}{z}\sum_{n=0}^{\infty}\left(\frac{1}{z}\right)^n \langle\phi_0|H_1^n|\phi_0\rangle , \tag{2.19}$$

and this expansion has a finite radius of convergence in $1/z$. The crux of the problem lies in the evaluation of vacuum expectation values of powers of the interaction H_1.

For an interaction of the form (2.12) the evaluation of matrix elements such as $\langle\phi_0|H_1^n|\phi_0\rangle$ has been treated in detail in many places. Using Wick's theorem,[9] each matrix element is given by a sum over contractions of the operators and can be put into one-to-one correspondence with Feynman-like diagrams. There are two basic types of diagrams: The connected diagrams are proportional to the volume of the system; the disconnected diagrams have a volume dependence depending upon the number of connected diagrams of which they are composed. A connected diagram is defined as one which cannot be divided into two separate parts without cutting at least one line. A disconnected diagram can be so divided.

If we let S_n denote the sum over all connected vacuum-to-vacuum graphs of order n, then $\langle\phi_0|H_1^n|\phi_0\rangle$ can be decomposed, following the analysis of one of us,[5] into products of connected graphs:

$$\langle\phi_0|H_1^n|\phi_0\rangle = g^n\Big(S_n + \sum_{\alpha+\beta=n} C^n_{\alpha\beta} S_\alpha S_\beta + \sum_{\alpha+\beta+\gamma=n} C^n_{\alpha\beta\gamma} S_\alpha S_\beta S_\gamma + \cdots + C_{11\ldots1}(S_1)^n\Big), \tag{2.20}$$

where the coefficients $C^n_{\alpha\beta}\ldots$ are given by

$$C^n_{\alpha_1\cdots\alpha_s} = \frac{1}{s!}\,\frac{n!}{\alpha_1!\alpha_2!\ldots\alpha_s!} . \tag{2.21}$$

It is shown in Ref. 5 that the resolvent operator can be written as

$$\langle R(z)\rangle_0 = \int_0^\infty dt\, e^{tz} e^{B_0(-gt)} , \tag{2.22}$$

where

$$B_0(-gt) = \sum_{n=1}^{\infty}\frac{S_n}{n!}(-gt)^n . \tag{2.23}$$

The integral representation (2.22) is valid for $\mathrm{Re}\,z < 0$. The function so defined can however be continued into the entire z plane. It then follows that

$$\langle\phi_0|U(-it)|\phi_0\rangle = \sum_m |\langle\phi_0|\psi_m\rangle|^2 e^{-E_m t} = e^{B_0(-gt)} . \tag{2.24}$$

$\langle\phi_0|\psi_m\rangle$ is the matrix element between the unperturbed vacuum and the mth eigenstate of the exact Hamiltonian. The asymptotic behavior of $B_0(-gt)$ as $t\to\infty$ must be dominated by a term linear in t:

$$B_0(-gt) \sim -\alpha t ,$$

where α is the lowest eigenvalue of H.

C. Convergence of Linked-Cluster Series

We observe that

$$\exp\Big(\sum_{n=1}^{\infty}\frac{S_n}{n!}(-gt)^n\Big) = \sum_m |\langle\phi_0|\psi_m\rangle|^2 e^{-E_m t} , \tag{2.25}$$

and the last is an entire function which increases as $|t|\to\infty$ no faster than $e^{\beta t}$ and thus is of order 1. By Hadamard's factorization theorem[10] an entire function $f(t)$ which is not zero at $t=0$ and which is of order 1 can be written in the form

$$f(t) = e^{Q(t)} P(t) , \tag{2.26}$$

where $Q(t)$ is a polynomial of degree not greater than 1 and $P(t)$ is the canonical product

$$P(t) = \prod_{n=0}^{\infty}(1 - t/t_n)\, e^{t/t_n} , \tag{2.27}$$

where the t_n are the zeros of $f(t)$.

If the series

$$B_0(-gt) = \sum_{n=1}^{\infty}\frac{S_n}{n!}(-gt)^n$$

had an infinite radius of convergence, $B_0(-gt)$ would be analytic in the entire t plane and e^{B_0} would have no zeros. Then the function

$$\sum_m |\langle\phi_0|\psi_m\rangle|^2 e^{-E_m t}$$

would have no zeros and, since it increases no faster than $e^{\beta t}$ as $|t|\to\infty$, it can, by the above argument, be written in the form

$$\sum_m |\langle\phi_0|\psi_m\rangle|^2 e^{-E_m t} = A\, e^{Bt} . \tag{2.28}$$

This gives a trivial result because it implies that the system possesses only one energy level. For nontrivial cases we conclude that $B_0(-gt)$ has a finite radius of convergence which immediately implies that the closely related series

$$\sum_{n=1}^{\infty} S_n (-gt)^n , \tag{2.29}$$

which for this model is essentially the Goldstone[11] series, has a zero radius of convergence. It is

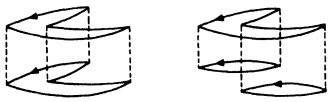

FIG. 2. Two fourth-order BCS diagrams.

shown further in Ref. 5 that the series (2.23) has a nonzero radius of convergence in t, a radius of convergence determined by the lowest zero of

$$\sum_m |\langle \phi_0 | \psi_m \rangle|^2 e^{-E_m t} .$$

D. Subsets of Graphs

For a many-fermion system it is usually not possible to find exact expressions for S_n. However, various subsets of graphs which are exactly or approximately calculable seem sometimes to dominate. One therefore hopes it will be possible by summing over such subsets to obtain meaningful results. One of the problems that can arise in doing this we discuss below.

Let us consider a system described by the BCS reduced Hamiltonian (in the strong-coupling limit):

$$H_{\mathrm{BCS}} = -V \sum_{\vec{k}\vec{k}'} c^*_{\vec{k}\uparrow} c^*_{-\vec{k}\downarrow} c_{-\vec{k}'\downarrow} c_{\vec{k}'\uparrow} .$$

This has a known exact solution[4] with ground state

$$E_0 = -(N^2 + N)V . \tag{2.30}$$

We now consider an attempt to obtain information using subsets of the totality of graphs generated by this Hamiltonian.

A diagram generated by the BCS reduced interaction Hamiltonian (2.13) is called a BCS diagram. Since H_{BCS} contains only a singlet interaction, a BCS diagram will divide into an upper and lower part with no solid lines connecting these parts as shown in Fig. 2. By convention the upper part represents the contractions of the spin-up operators; the lower part, the contractions of the spin-down operators. Figure 2(a) is an example of a ladder diagram, which is defined as a diagram where the upper part is identical to the lower part. In a nonladder diagram the spin-up part is connected together differently from the spin-down part. For the BCS case, as will be shown later, we find

$$S_n = N^n \left[S_n^{(0)} - \frac{1}{N} S_n^{(1)} + \frac{1}{N^2} S_n^{(2)} + \cdots \left(-\frac{1}{N}\right)^{n-2} S_n^{(n-2)} \right] , \tag{2.31}$$

where $S_n^{(0)}$, $S_n^{(1)}, \ldots$, are the number of certain subsets of the graphs generated by the BCS Hamiltonian to be defined later. $S_n^{(0)}$ is the number of ladder diagrams; this is easily shown to be

$$S_n^{(0)} = (n-1)! . \tag{2.32}$$

Examination of (2.31) suggests that one might attempt to approximate S_n in the limit that N becomes large by the ladder diagrams:

$$S_n \sim S_n^{(0)} N^n . \tag{2.33}$$

This was done by Fukushima and Fukuda[12] who approximated S_n generated by the BCS reduced Hamiltonian by the sum of all ladder diagrams neglecting all other contributions, arguing that they are at most of order $1/N$. If this approximation for S_n is now inserted into Eq. (2.23), one obtains

$$B_0(Vt) = -\ln(1 - NVt). \tag{2.34}$$

This gives an incorrect ground state for attractive potentials and displays the wrong asymptotic behavior; the result has been completely distorted by the approximation.

To discover what has gone wrong we note (the following is the argument of a previous publication[6]) that in this approximation $|\langle 0 | H^n_{\mathrm{BCS}} | 0 \rangle|$ is set equal to

$$|NV|^n S_n^{(0)} = |NV|^n (n-1)! . \tag{2.35}$$

On the other hand, if we consider all graphs,

$$\langle 0 | H^n_{\mathrm{BCS}} | 0 \rangle = \left\langle 0 \left| \left(V \sum_{\vec{k}\vec{k}'} c^*_{\vec{k}\uparrow} c^*_{-\vec{k}\downarrow} c_{-\vec{k}'\downarrow} c_{\vec{k}'\uparrow} \right)^n \right| 0 \right\rangle = V^n \sum_{\substack{\vec{k}_1 \ldots \vec{k}_n \\ \vec{k}'_1 \ldots \vec{k}'_n}} \langle 0 | c^*_{\vec{k}_1\uparrow} c^*_{-\vec{k}_1\downarrow} c_{-\vec{k}'_1\downarrow} c_{\vec{k}'_1\uparrow} \ldots c_{\vec{k}'_n\uparrow} | 0 \rangle . \tag{2.36}$$

Further since the vacuum expectation value of products of fermion operators satisfies the inequality

$$|\langle 0 | \ldots c \ldots c^* \ldots | 0 \rangle| \leq 1 , \tag{2.37}$$

then

$$|\langle 0 | H^n_{\mathrm{BCS}} | 0 \rangle| < |V^n| \sum_{\substack{\vec{k}_1 \ldots \vec{k}_n \\ \vec{k}'_1 \ldots \vec{k}'_n}} 1 = 4 |VN^2|^n . \tag{2.38}$$

If we compare this result with that obtained by considering only ladder diagrams (2.35), we see that for n large enough

$$(n-1)! > 4N^n ,$$

which means that the subset of ladder graphs does not correspond to an actual Hamiltonian.

Looking more closely at the diagrammatic analysis, we discover what is wrong. The evaluation of $\langle 0 | H^n_{\mathrm{BCS}} | 0 \rangle$ by means of Wick's theorem usually involves summations over indices attached to intermediate particle or hole lines disregarding restrictions imposed by the exclusion principle. We are therefore obliged to include a large number of processes apparently violating this principle so that the violation may be cancelled out as a whole.

This point has been stressed by Goldstone[11] as extremely important if the linked-cluster expansion is used.

In the fourth order, for example, we see that the graphs shown in Fig. 2(a), which are included in $S_4^{(0)}$, may violate the Pauli exclusion principle in the intermediate states. However, since all the graphs included in $S_n^{(0)}$ are positive, there is no possible way they can be cancelled. A diagram that contributes to the wanted cancellation, Fig. 2(b), is neglected in the ladder approximation. This diagram gives a contribution $-N^3$ compared with N^4 for a ladder diagram, but the number of this type increases rapidly with n, all adding up to a contribution which cannot be neglected. [Our analysis of the BCS graphs indicates that the ladder graphs dominate only as long as $n \lesssim (3N)^{1/2}$.]

E. Criterion for Validity of Many-Body Approximations

The results obtained above show that the difficulties encountered in attempting to approximate S_n of (2.31) arise due to the inclusion of a very large number of uncancelled exclusion-principle-violating processes (following Kelly,[13] hereafter abbreviated EPV processes) in higher-order terms of the expansion. This suggests that an approximation used in the analysis of many-body systems which leads to the inclusion of large numbers of EPV processes, in the absence of evidence to the contrary, should be regarded with suspicion.

This has led us, in a previous publication, to propose as one criterion for the validity of an approximation to a many-body system that it not result in the inclusion of large numbers of uncancelled terms that violate the exclusion principle. One method of achieving this is via what we have called the proper completion.

Let $\{S_n^{(a)}\}$ be some approximation to the full set of connected graphs. We define a new function

$$\langle 0|\, U^{(a)}(-it)\,|0\rangle_{EP} = \exp\left(\sum_{n=1}^{\infty} \frac{S_n^{(a)}}{n!}(-gt)^n\right) - S_{EPV} \ . \tag{2.39}$$

where S_{EPV} denotes all contributions from exclusion-principle-violating processes. The subscript EP indicates that the new function contains no EPV processes. Given the set of graphs $\{S_n^{(a)}\}$, suppose we can add to it another set $\{S_n^{(b)}\}$ with the following properties: (i) Every process represented by the graphs $\{S_n^{(b)}\}$ violates the exclusion principle. (ii) The final result contains no EPV processes. It then follows that

$$\exp\left(\sum_{n=1}^{\infty} \frac{S_n^{(a)}+S_n^{(b)}}{n!}(-gt)^n\right) = \langle 0|\, U^{(a)}(-it)\,|0\rangle_{EP} \ , \tag{2.40}$$

and we may calculate in the usual manner with the new set of graphs. We call the set $\{S_n^{(b)}\}$ the *proper completion* of $\{S_n^{(a)}\}$.

We are thus led, having chosen a subset of $\{S_n^{(a)}\}$ on the basis perhaps of a small parameter, to add to this a subset $\{S_n^{(b)}\}$ as defined above with no reference to this parameter. When this is done the properly completed subset $\{S_n^{(a)}+S_n^{(b)}\}$ will yield an approximate U matrix by the usual formula. Any set of connected graphs generated by a Hamiltonian (no matter how truncated) will have the property of yielding a U matrix which contains no exclusion-principle-violating processes. Thus we may view the process of proper completion as a process which converts an arbitrary set of graphs into one which might come from a Hamiltonian. Since the BCS graphs, as has been shown in Ref. 6, are either ladder or EPV graphs, the BCS reduced Hamiltonian can be viewed as resulting from the proper completion of the ladder graphs.

A less exacting requirement follows. If again $\{S_n^{(a)}\}$ is some approximation to the full set of connected graphs characterized as being of some order in a small parameter, we can approximate the function (2.39) by adding to $\{S_n^{(a)}\}$ another set $\{S_n^{(c)}\}$ such that (i) all graphs of $\{S_n^{(c)}\}$ are of higher order than $\{S_n^{(a)}\}$ and (ii) the final result contains no EPV processes. It then follows that

$$\exp\left(\sum_{n=1}^{\infty} \frac{S_n^{(a)}+S_n^{(c)}}{n!}(-gt)^n\right) = \langle \phi_0|\, U^{(a)}(-it)\,|\phi_0\rangle_{EP} \tag{2.41}$$

to the same order in the small parameter as the graphs $S_n^{(a)}$. The set $\{S_n^{(a)}+S_n^{(c)}\}$ we call a completion of $S_n^{(a)}$.

One of the difficulties in many-body theory of this type is to find a parameter which is small and in which some expansion can be made. The situation is confused by the necessity of including contributions of higher order in this parameter in order that the analysis be consistent. Although there is fairly general agreement that $N \to \infty$ cannot be taken too easily in any calculation, the same difficulty can be encountered, as we shall see later, with parameters that are apparently independent of the number of particles or the volume of the sample.

III. GENERALIZED BCS (GBCS) HAMILTONIAN

A. Definition

Although the Hamiltonian (2.12)

$$H_1 = g \sum_{\vec{k},\vec{k}',\vec{q}} c^*_{\vec{k}+\vec{q}\uparrow}\, c^*_{\vec{k}'-\vec{q}\downarrow}\, c_{\vec{k}'\downarrow}\, c_{\vec{k}\uparrow}$$

retains most of the complexity of many-body dynamics, it has been so shorn of (what we hope to be) irrelevant difficulties that only two problems remain: the exclusion principle and the phase sums introduced at each vertex due to momentum conservation and the restriction of all states to the thin shell surrounding the Fermi surface. We now

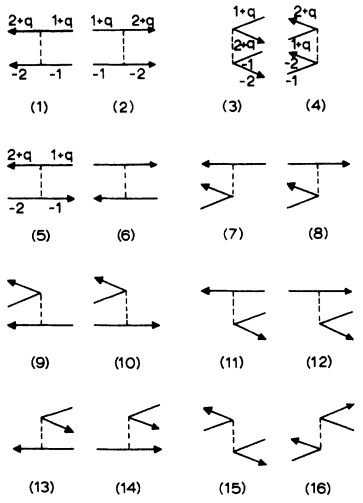

FIG. 3. (1), (2), (3), and (4) are the BCS vertices; the others are not generated by the BCS Hamiltonian.

ask if there is some consistent manner in which we can begin with (2.12) and arrive at the results of the BCS Hamiltonian (2.13).

A graph generated by the Hamiltonian (2.12) may be constructed from any of 16 vertices produced by the two-body interaction shown in Fig. 3. By convention the upper part of a vertex represents particles with spin up and lower part represents particles with spin down. The BCS Hamiltonian picks out of these 16 vertices just four which are labelled (1) to (4). We call them the BCS-type vertices. Any graph which we cannot construct from these four vertices is not generated by the Hamiltonian (2.13). For example, in Fig. 4, graph (a) is not of the BCS type whereas graphs (b), (c), and (d) are. In addition to this topological restriction, each graph of the BCS type couples only electron lines of opposite spin and momentum.

To analyze the phase-space sums, we consider first the BCS-type vertices [Fig. 3, (1)–(4)]. If we fix the incoming momentum $\vec{1}$, the available phase space for scattering is seen to be a function $N_1(q)$ strongly dependent on the magnitude of the total momentum a of the incoming pair. The maximum phase space available for scattering (and thus the maximum weight for the vertex) will occur when $q=0$. As q departs from zero, the available phase space decreases rapidly as shown in Fig. 5. All of the BCS-type vertices depend upon q in the same manner. As the interaction shell grows thinner ($\delta/k_F \to 0$), the phase-space curve grows sharper and sharper and comes closer and closer to the $(\vec{k}\uparrow, -\vec{k}\downarrow)$ pairing.

The 12 remaining vertices are not of the BCS type; these contribute a phase-space sum $M_1(q)$ of Fig. 5 which goes to zero as $q \to 0$, reaches a maximum at $q \approx (2\delta)^{1/2}$, and then decreases in the same

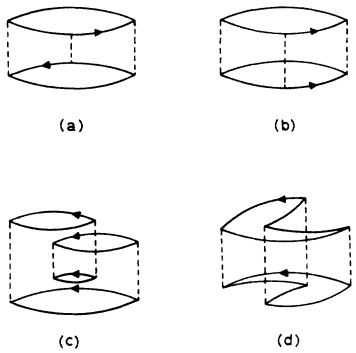

FIG. 4. Graph (a) is not of the BCS type whereas (b), (c), and (d) are.

manner as $N_1(q)$ from $q=2\delta$. Hence they contribute less than the particle-particle processes. What is more significant, they contribute according to another (smaller) coupling constant than all of the particle-particle or hole-hole processes—those generated by the four BCS-type vertices—and their contribution goes to zero as the momentum of the scattering pair goes to zero.

Thus the graphs generated solely from the vertices (1)–(4) are distinguished from the totality of graphs generated by the strongly coupled Hamiltonian in that they contain contributions when the momentum of the pairs being scattered approaches zero. Since we are particularly interested in the scattering of electron pairs of small (but not necessarily zero) total momentum, these are the graphs that dominate.

Guided by this we consider what we call the generalized BCS (GBCS) Hamiltonian, a Hamiltonian which generates all the graphs produced by the BCS-type vertices (1)–(4) of Fig. 3. If we use $h_{\vec{k}\sigma}$ and $p_{\vec{k}\sigma}$, respectively, for hole and particle operators as referred to our vacuum, we may write

$$H_{\mathrm{GBCS}} = -V \sum_{\vec{k},\vec{k}',\vec{q}} \{ p^*_{\vec{k}+\vec{q}\uparrow}\, p^*_{\vec{k}'-\vec{q}\downarrow}\, p_{\vec{k}'\downarrow}\, p_{\vec{k}\uparrow} + h_{\vec{k}+\vec{q}\uparrow}\, h_{\vec{k}'-\vec{q}\downarrow}\, h^*_{\vec{k}'\downarrow}\, h^*_{\vec{k}\uparrow} + h_{\vec{k}+\vec{q}\uparrow}\, h_{\vec{k}'-\vec{q}\downarrow}\, p_{\vec{k}'\downarrow}\, p_{\vec{k}\uparrow} + p^*_{\vec{k}+\vec{q}\uparrow}\, p^*_{\vec{k}'-\vec{q}\downarrow}\, h^*_{\vec{k}'\downarrow}\, h^*_{\vec{k}\uparrow} \} \,. \quad (3.1)$$

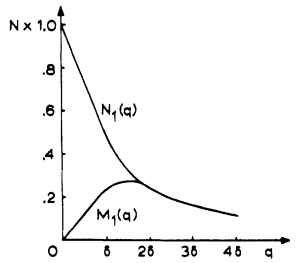

FIG. 5. Phase-space weight as a function of pair momentum q.

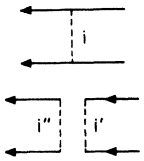

FIG. 6. Gaudin's decomposition of a two-body vertex.

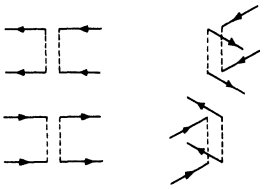

FIG. 7. Gaudin decomposition of the BCS-type vertices.

From this Hamiltonian we obtain a set of graphs topologically identical to the BCS set, but not restricted to $(\vec{k}\uparrow, -\vec{k}\downarrow)$ pairing. The GBCS Hamiltonian may therefore be considered the most natural generalization of the BCS reduced Hamiltonian.

The dominance of low-momentum pair scattering is a consequence of the smallness of δ/k_F. What we believe is the relevant natural parameter of the problem (later called Q/N) is proportional to $(\delta/k_F)^2$ and is independent of the number of particles or the volume of the system. Of the graphs generated by the Hamiltonian (2.12), the ladder graphs are of lowest order in this parameter. One is thus tempted to extract these graphs and use them as the leading term in some approximation. However, using the subset of ladder graphs to approximate S_n leads to the same meaningless results as in the BCS case discussed in Sec. II and for the same reasons. The GBCS Hamiltonian (3.1) may be viewed as a completion of the ladder graphs generated by (2.12) in the sense discussed at the conclusion of Sec. II. The total set of graphs generated by (3.1) does not give any uncancelled exclusion-principle-violating processes while adding no graphs of as low an order in $(\delta/k_F)^2$ as the ladder graphs. We may thus regard the GBCS Hamiltonian (3.1), which is a natural generalization of the BCS Hamiltonian, as resulting from the completion of the ladder graphs generated by the full strongly coupled Hamiltonian (2.12).

B. Gaudin's Cycle Decomposition

To determine the sum over the connected graphs, S_n, generated by the GBCS Hamiltonian we must (i) find all the topologically nonequivalent diagrams of order n, (ii) determine the sign of a given diagram, (iii) determine the weight of that diagram, and (iv) sum the contributions of such connected nth-order diagrams.

We attempt to do this using a method of graphical decomposition first introduced by Gaudin[14] for handling summations over a spin variable; the treatment of the GBCS diagrams becomes particularly transparent with this technique.

According to Gaudin a two-body vertex i is decomposed into two separate parts which we label i'' and i'. This is shown in Fig. 6. The parts i'' and i' represent, respectively, the creation and annihilation operators. All of the graphs with the BCS topology can be constructed from Gaudin vertices for which both the lines leaving i'' or entering i' go in the same direction. This would not be true for a general two-body vertex. The condition that both of the incoming and outgoing lines be either particle or hole lines defines the BCS-type vertices (1)–(4) of Fig. 3. This is shown in Fig. 7. We emphasize that the GBCS diagrams are topologically identical to those generated by the BCS Hamiltonian. Thus the cyclic decomposition of the graphs generated by these two Hamiltonians is identical.

A line leaving a vertex part i'' must end at a part j'. A diagram analyzed in this way will be decomposed into a certain number of cycles. An example of this is shown in Fig. 8, where a fourth-order GBCS diagram is decomposed into the cycles γ_a, γ_b, and γ_c. As a result of the topology of the BCS-type vertices, a single cycle will be made entirely of particle lines or hole lines as there is no mixing of particles and holes in a single cycle. The decoupling of a diagram is unique; once the diagram is given so are the cycles; or if we specify the cycles and their relative positions, the diagram is completely determined.

The simplest cycles are those of the type γ_b and γ_c in Fig. 8. We call them elementary cycles. A ladder diagram is defined as a diagram where the upper part is identical to the lower part as illustrated in Fig. 9 and is composed solely of elementary cycles. We further observe that an nth-order ladder diagram consists of n cycles which is the maximum number of cycles into which any diagram may be decomposed.

For any diagram other than a ladder, at least one cycle is not of the elementary type; therefore, a nonladder diagram will consist of less than n cycles. Since any connected diagram, excluding

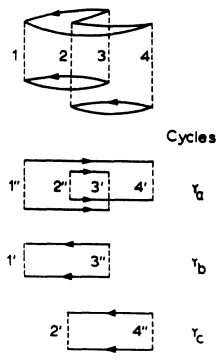

FIG. 8. Decomposition of a fourth-order diagram.

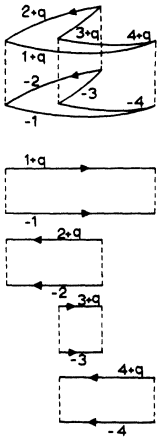

FIG. 9. Decomposition of a fourth-order ladder diagram.

first order, consists of at least one hole and one particle line, two is the smallest number of cycles.

To simplify the counting, scattering processes with zero momentum transfer are included, corresponding to the presence of diagonal terms in the Hamiltonian. Such processes lead to a class of nonladder diagrams in which a hole line goes back to the same vertex from which it started. Such a part (called by Goldstone a passive unexcited particle loop) comes from the contraction $:h_{k_i\sigma}h^*_{k_i\sigma}:$; we will call it a bubble. An example of the decomposition of a diagram containing a bubble is shown in Fig. 10.

The sign of a diagram is uniquely determined by its topology; with the cycle analysis the sign of a given diagram may be written[14] as

$$(-1)^{n+f}\ , \tag{3.2}$$

where f (which goes from n to 2) is the number of cycles of which the diagram is composed. It is important to note that all contributions from nth-order diagrams with the same number of cycles will have the same sign. This is one of the reasons that the classification of the connected diagrams according to the number of cycles is useful.

Before attempting to evaluate the sum of nth-order connected GBCS diagrams, we shall demonstrate how the cycle analysis can be used to find the corresponding sum of the BCS diagrams. We note that in the limit that the pair momentum $\vec{q}\to 0$, these two sums of diagrams must be equal.

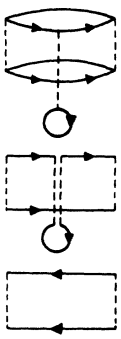

FIG. 10. Decomposition of a diagram with a bubble.

C. Cycle Analysis of BCS Diagrams

Application of the cycle analysis to the strongly coupled BCS Hamiltonian (2.13) reveals that the weight of any BCS graph is given entirely by the number of cycles into which it is decomposed. Consider the ladder graph Fig. 9. In order that this be a BCS graph, $\vec{q}=0$. Then all of the electrons are in $(-\vec{i}\downarrow, \vec{i}\uparrow)$ pairs. The weight of this graph is just the sum over the momenta $\vec{1}$, $\vec{2}$, $\vec{3}$, and $\vec{4}$ with the restriction that these momenta lie in either the particle or hole shell. Since $\vec{1}$, $\vec{2}$, $\vec{3}$, and $\vec{4}$ are independent of one another, the summation gives immediately

$$\sum_{\vec{1},\vec{2},\vec{3},\vec{4}} 1 = N^4\ .$$

As the interaction shell has the same number of particle and hole states, it is irrelevant in the summation whether we have contractions of hole or particle operators. At this point the advantage of including processes with zero momentum transfer becomes clear: All free indices have the same number N of possible values.

The weight of this graph is N^4 and its sign is $(-1)^{n+f}=(-1)^{4+4}=1$. The graph therefore contributes $+N^4$. In the same manner we can easily show that any ladder graph in the nth order is decomposed into n cycles each of which yields a free index $\vec{i}$ ($\vec{1}$, $\vec{2}$, $\vec{3}$, and $\vec{4}$ above). Thus the total contribution of such a graph is N^n. There are $(n-1)!$ ladder graphs of the nth order. Therefore as has been mentioned before (2.32), we get

$$S_n^{\text{LADDER}} = (n-1)!\,N^n\ . \tag{3.3}$$

We now consider a nonladder graph such as that shown for example in Fig. 8. The cycle decomposition with the BCS labelling is shown in Fig. 11. Due to the pairing condition each cycle is labelled by one and only one free index ($\vec{i}=\vec{1}$, $\vec{2}$, and $\vec{3}$). The number of free indices in a BCS diagram is in general simply the number of cycles, f, into which the diagram can be decomposed. Hence the weight

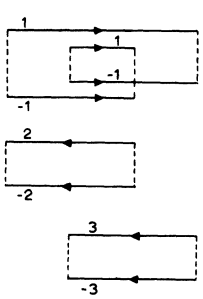

FIG. 11. Cyclic decomposition of a fourth-order BCS graph.

factor W_n for an nth-order BCS diagram is

$$W_n^{\mathrm{BCS}} = N^f \ . \tag{3.4}$$

We notice that a cycle connecting more than two vertices will be characteristic of all but the ladder diagrams. Such cycles represent EPV processes. Hence we may conclude that all nonladder BCS diagrams violate statistics. The BCS diagrams may therefore be classified as either ladder or EPV diagrams.

The total contribution (weight factor and sign) of an nth-order connected BCS diagram is

$$(-1)^{n+f} N^f \ . \tag{3.5}$$

And, as was stated in (2.31), the sum of nth-order connected BCS diagrams is

$$S_n = N^n \left[S_n^{(0)} - \frac{1}{N} S_n^{(1)} + \frac{1}{N^2} S_n^{(2)} \cdots \left(-\frac{1}{N} \right)^{n-2} S_n^{(n-2)} \right] ,$$

where the positive integers, $S_n^{(\alpha)}$, are now defined as the number of connected graphs of the BCS topology of order n with $n-\alpha$ cycles. As will be shown later, the $S_n^{(\alpha)}$ can be obtained through a detailed study of the possible combinations of the BCS cycles. All BCS diagrams containing a certain number of cycles have the same sign and the same weight factor. Each graph can therefore be characterized by the degree to which it deviates from a ladder graph. A pure BCS ladder graph of the nth order has the weight N^n while the related nth-order BCS graph containing $n-\alpha$ cycles (where α is no larger than $n-2$) has the weight

$$N^n (1/N)^\alpha \ . \tag{3.6}$$

We observe further that if any other of the unperturbed states, $|\phi_i\rangle$, had been used as the vacuum, H_{BCS} would retain its form and all the diagrams would be the same. The summation over the intermediate states would result in the same sums over independent indices as each $\vec{k}\uparrow$ is coupled only to $-\vec{k}\downarrow$. These sums depend solely upon the number of hole and particle single-particle states, which are the same for all $|\phi_i\rangle$ since the number of particles in the interaction shell is constant. Therefore S_n is independent of which unperturbed state is used as the vacuum.

D. Convention for Labelling GBCS Cycles

We have seen that any graph can be decomposed uniquely into cycles; each cycle is characterized by a principal momentum $\vec{i} = \vec{1}, \vec{2}, \vec{3} \ldots \vec{f}$ and by the pair momenta $\vec{q}_1 \ldots \vec{q}_s$, where s is the number of vertices connected by the cycle. We label the lines of a cycle as follows. The first lower line on the left (going from left to right) is given the momentum $-\vec{i}$. The upper line with which it interacts on the left is labelled $\vec{i}+\vec{q}_1$ (thus the total momentum of this pair is $\vec{q}_1$). The lower line with which $\vec{i}+\vec{q}_1$ interacts on the right (termination for both of them) is labelled $-\vec{i}-\vec{q}_1-\vec{q}_2$ (thus momentum $-\vec{q}_2$ for this pair). In this way one can go through the entire cycle until the last line, which is the continuation of the first, is labelled with the momentum $-\vec{i}-\vec{q}_1-\vec{q}_2-\cdots\vec{q}_s$.

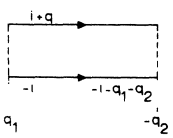

FIG. 12. An elementary cycle.

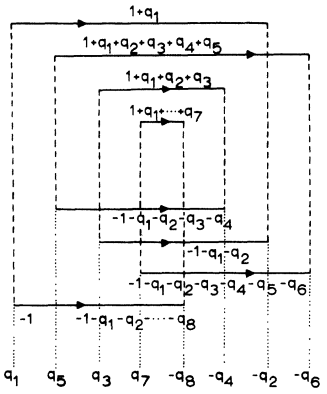

FIG. 13. Cycle connecting eight vertices.

For an elementary cycle, see Fig. 12, there are two momenta $\vec{q}_1$ and $\vec{q}_2$; these satisfy the condition

$$\vec{q}_1 + \vec{q}_2 = 0 \quad \text{or} \quad \vec{q}_1 = -\vec{q}_2 \ .$$

Thus there is only one independent momentum. More complicated cycles are characterized by the pair momenta $\vec{q}_1 \ldots \vec{q}_s$. Only $(s-1)$ of these are independent. This is demonstrated in Fig. 13, where a BCS-type cycle with the principle momentum $\vec{1}$ and the pair momenta $\vec{q}_1\, \vec{q}_2 \ldots \vec{q}_8$ is shown. Any cycle labelled in this manner gives a condition on the pair momenta,

$$\vec{q}_1 + \vec{q}_2 + \vec{q}_3 + \cdots + \vec{q}_s = 0 \ .$$

Thus the two apparently different labellings of the bottom line are the same. If each of the pair momenta is zero, one has exact pairing or a BCS cycle.

E. Polygon Weight Factors for Phase-Space Sums

The GBCS Hamiltonian differs from the BCS Hamiltonian in that the particles or holes are no longer paired $(-\vec{i}\downarrow, \vec{i}\uparrow)$. It thus permits the interaction of an electron $-\vec{i}\downarrow$ with all electrons $\vec{i}+\vec{q}\uparrow$. Any "pairing" must therefore be the result of the dynamics which for this model are contained in the phase-space summations. These are dominated by the requirement that the total momentum of any in-

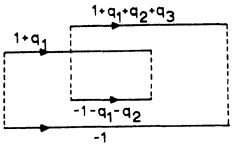

FIG. 14. Cycle connecting four vertices.

teracting pair be small enough so that there remains a substantial volume of phase space into which transitions can take place. From the function $N_1(q)$ in Fig. 5 it is clear that large values of $N_1(q)$ and hence large weight factors only exist if $-\vec{i}\downarrow$ and $\vec{i}+\vec{q}\uparrow$ are nearly paired.

Because $N_1(q)$ is peaked sharply at $q=0$, scattering of zero-momentum pairs becomes dominant in higher orders. For an nth-order ladder graph, for example, one encounters terms of the form

$$N\sum_q [N_1(q)]^{n-1} .$$

In sufficiently high order only the $q=0$ term will contribute.

While this extreme dominance of the scattering by the $q=0$ term in high order seems to be a fact, it is exaggerated by the factor $N_1(q)$ as obtained from the intersecting shells of the strongly coupled model. The long tail of $N_1(q)$ which contributes to the scattering only in the lowest orders is likely also to be of no more general significance since, for the states of large $\vec{q}$, $(\vec{i}+\vec{q}\uparrow)$ probably do not interact strongly with $-\vec{i}\downarrow$ and can be treated as a perturbation. However, it is difficult to see why $\vec{i}\downarrow$ should be strongly preferred to $+\vec{I}+\vec{q}\uparrow$ if $|\vec{q}|\lesssim\delta$.

We have for this reason chosen to lessen the peaking of $N_1(q)$ and eliminate the tail in a model in which $N_1(q)$ is replaced by a constant $N_1(0)=N$ for a region Q of phase space centered about $\vec{q}=0$:

$$N_1(q)=N\,, \quad |\vec{q}|\leq q_0$$
$$=0\,, \quad \text{otherwise}$$

where

$$Q=\sum_{|\vec{q}|<q_0} 1=\frac{\Omega}{2\pi^2}\frac{{q_0}^3}{3} . \tag{3.7}$$

The maximum momentum q_0 is of the order of δ so that

$$Q\sim\delta^3$$

and the expansion parameter

$$\frac{Q}{N}=\frac{{q_0}^3/3}{{k_F}^2\delta}\sim\left(\frac{\delta}{k_F}\right)^2 . \tag{3.8}$$

In this model we allow the electron $-\vec{i}\downarrow$ to interact with the same weight with any given electron in the sphere of phase volume Q centered at $\vec{i}\uparrow$. We thus exaggerate the interaction of $-\vec{i}\downarrow$ with those electrons not exactly paired to it in order to see if this destroys the qualitative results associated with the pairing Hamiltonian.

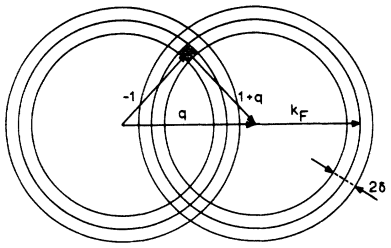

FIG. 15. Construction giving $N_1(q)$.

The phase sum associated with any cycle is the sum over all $\vec{1}$, $\vec{q}_1$, $\vec{q}_2\ldots\vec{q}_s$ such that the momenta $-\vec{1}$, $+\vec{1}+\vec{q}_1$, $-\vec{1}-\vec{q}_1-\vec{q}_2\cdots$, $\vec{1}+\vec{q}_1+\vec{q}_2+\cdots\vec{q}_s$ are each in the interaction shell.

Consider a cycle with four vertices as shown in Fig. 14. Here the sum is to be taken over all $\vec{1}$, $\vec{q}_1$, $\vec{q}_2$, and $\vec{q}_3$ such that $-\vec{1}$, $\vec{1}+\vec{q}_1$, $-\vec{1}-\vec{q}_1-\vec{q}_2$, and $\vec{1}+\vec{q}_1+\vec{q}_2+\vec{q}_3$ all are within the shell of interaction. The first momentum (labelled by the arabic numeral $-\vec{1}$ in this case) can be chosen freely from any of the N hole states of spin $\downarrow$. The second is restricted by the condition of intersecting shells as shown in Fig. 15.

The third momentum $(-\vec{1}-\vec{q}_1-\vec{q}_2)$ must be in the interaction shell at the same time as $\vec{1}+\vec{q}_1$. If these were the only two involved, the condition would be given by the intersection volume of two shells separated by $\vec{q}_2$. However, $-\vec{1}$ must also be in the shell. Thus the momenta which simultaneously satisfy the condition that $-\vec{1}$, $\vec{1}+\vec{q}_1$, and $-\vec{1}-\vec{q}_1-\vec{q}_2$ all be in the interaction shell are given by the intersection of three shells: the second separated from the first by $\vec{q}_1$ and the third separated from the second by $+\vec{q}_2$ (see Fig. 16). Unless $\vec{q}_1+\vec{q}_2$ is small the volume of intersection goes rapidly to zero.

The fourth momentum $\vec{1}+\vec{q}_1+\vec{q}_2+\vec{q}_3$ must also be in the interaction shell. Thus (referring to $-\vec{1}-\vec{q}_1-\vec{q}_2$) it will be in the intersection of two shells separated by $\vec{q}_3$. All of the conditions are satisfied by the volume of intersection of the shells whose centers are separated by $\vec{q}_1$, $\vec{q}_2$, and $\vec{q}_3$ (see Fig. 17). Given this we see that the shell centered

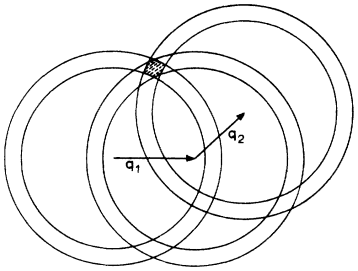

FIG. 16. Exaggerated drawing of three intersecting shells.

at D must intersect that centered at A as well as that at C and that at B. This guarantees that the two momenta $\vec{1}+\vec{q}_1+\vec{q}_2+\vec{q}_3$ and $-\vec{1}$ also lie within the interaction shells; in general, the intersection region is *symmetrical* in all of the momenta. The phase polygon for the more complicated cycle of Fig. 13 is shown in Fig. 18.

We write the phase sum associated with a cycle of $s+1$ vertices as

$$N_s(\vec{q}_1 \ldots \vec{q}_s) \ . \tag{3.9}$$

For the ladder cycle (which has two vertices) this reduces to our original $N_1(q)$ which as discussed before is the phase space which is the intersection volume of the two shells—and is a ring (or perhaps more accurately a slightly flat radial tire) which for $\delta < q < 2k_F$ has the volume

$$N_1(q) \sim N\delta/2q \ . \tag{3.10}$$

The function $N_2(\vec{q}_1\vec{q}_2)$ is the intersection volume of the three shells of Fig. 16. The intersection of any two of these gives a radial tire whose plane bisects the momenta ($\vec{q}_1$, $\vec{q}_2$, or $\vec{q}_3$) and is perpendicular to it.

Generally the intersection volume of the radial tires is zero for most values of $q > \delta$ and for those few values of $\vec{q}_1 \ldots \vec{q}_s$ for which it is not zero, of the order of δ^3. If all values of the pair momenta except one, $\vec{q}$, are very small, (3.9) becomes essentially $N_1(q)$. With (3.7), $N_1(q)$ is written as

$$\begin{aligned} N_1(q) &= N, \quad |q| \leq q_0 \\ &= 0, \quad \text{otherwise} ; \end{aligned} \tag{3.11}$$

a similar approximation gives for the $s+1$ point function

$$\begin{aligned} N_s(\vec{q}_1 \ldots \vec{q}_s) &= N , \quad \text{if the maximum distance between any of the } s+1 \text{ points of the phase polygon is no larger than } q_0 \\ &= 0 , \quad \text{otherwise} . \end{aligned} \tag{3.12}$$

An estimate of the magnitude of the summation over pair momenta for a cycle with $s+1$ vertices

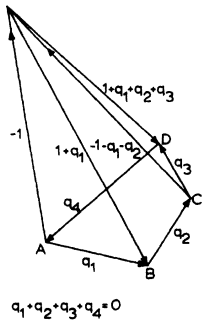

FIG. 17. Phase-space polygon for the cycle shown in Fig. 14.

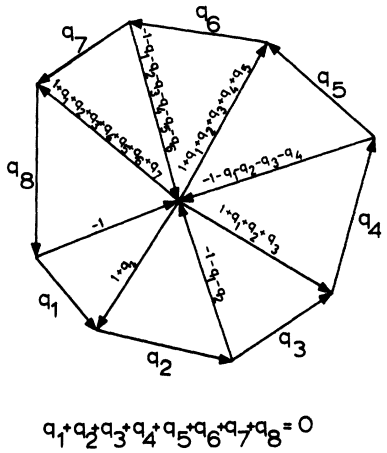

FIG. 18. Exaggerated eight-point phase polygon.

$$\sum_{\vec{q}_1 \cdots \vec{q}_s} N_s(\vec{q}_1 \ldots \vec{q}_s) \tag{3.13}$$

can be obtained by treating the variables $\vec{q}_i$ as in a random walk and replacing the condition (3.12) by the average condition that

$$\langle \vec{q}^{\,2} \rangle_{av} = \left\langle \left(\sum_{i=1}^{s} \vec{q}_i \right)^2 \right\rangle_{av} \leq q_0^2 . \tag{3.14}$$

We then obtain

$$\sum_{\vec{q}_1 \cdots \vec{q}_s} N_s(\vec{q}_1 \cdots \vec{q}_s) = N Q_{(s)}^s , \tag{3.15}$$

where

$$Q_{(s)} = Q/s^{3/2} \tag{3.16}$$

and Q is defined by (3.7).

F. Cycle Linkage and Reduced Polygons

We have so far analyzed individual cycles. Any graph however is composed of two or more cycles whose momenta are related to one another due to the conservation of total momentum at each vertex; thus the weight of a GBCS graph composed of several cycles will depend upon the manner in which the cycles are linked together. There is an intrinsic quasipairing in the scattering at each vertex due to the phase-space function $N_1(q)$ [approximated, for example, by (3.7)] so that it remains convenient to label each cycle by one principal momentum; the additional momenta are, as we have seen, the pair momenta $\vec{q}_1$, $\vec{q}_2 \ldots$.

Consider the ladder graph shown in Fig. 19. All pair momenta must be equal if total momentum is conserved at each vertex; hence,

$$\vec{q}_1 = \vec{q}_2 = \vec{q}_3 = \vec{q}_4 \ .$$

The complete labelling of this graph is shown in Fig. 9. There are altogether $n+1 = 4+1 = 5$ indices. Looking next at the nonladder graph shown in Fig.

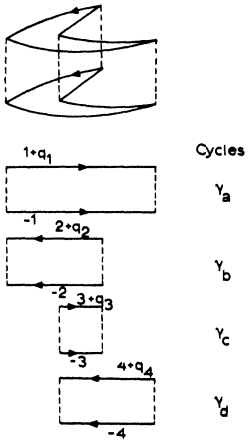

FIG. 19. Redundant pair momenta in elementary cycles before conservation of momentum is imposed.

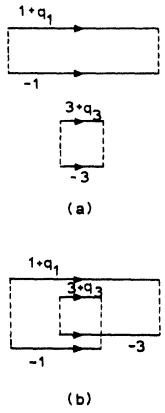

FIG. 21. Construction of a nonelementary cycle (b) from two elementary cycles (a).

20, we observe that two $\vec{q}$ indices are now needed to label the diagram. At the same time the number of principal momenta is reduced by one. The total number of indices needed to label nth-order graphs in general is $n+1$.

This may perhaps most easily be seen as follows. The difference between the ladder and nonladder graphs in Fig. 19 and Fig. 20 is the way the spin-down hole lines are connected. The nonladder graph can actually be obtained from the ladder graph if the vertices in cycle γ_a and γ_c are connected by the spin-down lines as shown in Fig. 21. Comparing the resulting cycle with the same cycle shown in Fig. 20, we see that the momentum indices must satisfy the equation

$$\vec{3}+\vec{q}_3=\vec{1}+\vec{q}_1$$

or

$$\vec{3}=\vec{1}+\vec{q}_1-\vec{q}_3 \quad . \tag{3.17}$$

As a result there is one less principal momentum but one more pair momentum, $\vec{q}$, in the phase-space sum. Similar arguments apply for all graphs.

From this it is clear that associating one principal momentum $\vec{1}$ and v pair momenta $\vec{q}_1 \ldots \vec{q}_v$ to each cycle with v vertices results in a redundant number of momenta. For each cycle we have the condition

$$\vec{q}_1+\vec{q}_2+\cdots\vec{q}_v=0 \tag{3.18}$$

and at each vertex a condition from conservation of momentum (see Fig. 20). The use of these conditions for any nth-order connected graph composed of f cycles leaves us with the f principal momenta

$$\vec{1}_1 \ldots \vec{1}_f \tag{3.19}$$

and $n-f+1$ pair momenta

$$\vec{q}_1 \ldots \vec{q}_{n-f+1} \tag{3.20}$$

now distributed among the f cycles. The total weight of a graph is therefore given by the product of phase polygons obtained for each cycle with the number of pair momenta reduced to its proper value. Phase polygons for which such a reduction has been carried out are called reduced polygons. We now discuss the method of reduction and of obtaining the total weight.

In Fig. 22 the cycles of the nonladder graph of Fig. 20 are shown labelled. The original polygons for these cycles are shown in Fig. 23(a). Requiring conservation of momentum at each vertex, we now find

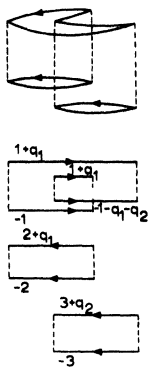

FIG. 20. Cycle analysis of a nonladder GBCS diagram.

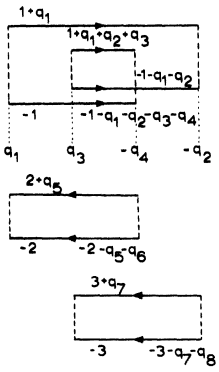

FIG. 22. Three cycles containing redundant pair momenta.

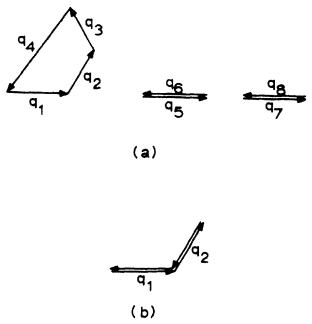

FIG. 23. Original polygons (a) and reduced polygon (b) for the cycles of Fig. 22.

$$\vec{q}_1 = -\vec{q}_4\ ,\quad \vec{q}_3 = -\vec{q}_2\ ,$$
$$\vec{q}_5 = \vec{q}_1\ ,\quad \vec{q}_7 = \vec{q}_3\ . \tag{3.21}$$

This reduces the four-point phase polygon to the three-point polygon shown in Fig. 23(b). Since $\vec{q}_5 = \vec{q}_1$ and $-\vec{q}_7 = \vec{q}_2$, the restrictions implicit in the two-point polygons of Fig. 23(a) are already contained in the three-point polygon, which restricts permissible $\vec{q}$ values more severely than the two-point polygon. The two-point polygons therefore add no new restriction so that the total weight is given by the three-point reduced polygon. [The important idea is that if a pair momentum occurs in two polygons, one with a larger number of vertices than the other, the sum over this pair momentum (restricted in any case to $|q| \leq q_0$) is more restricted by the larger polygon than the smaller. Thus any restriction imposed by the smaller polygon is redundant. If the two polygons have the same number of vertices, the restriction imposed by one is duplicated by the other.] Using this technique the weight factor for any GBCS graph can be obtained.

The ladder diagrams for example are characterized by n principal momenta and one pair momentum. Using (3.7), the summation over phase space therefore gives

$$\sum_{\substack{-\vec{1},-\vec{2},\cdots-\vec{n},\vec{q}\\ \vec{1}+\vec{q},\vec{2}+\vec{q}\cdots\vec{n}+\vec{q}\\ \text{all in shell}}} 1 = N\sum_{q}\left[N_1(q)\right]^{n-1}$$
$$= N^n \sum_{|\vec{q}|\leq q_0} 1 = QN^n\ . \tag{3.22}$$

The nonladder graph of Fig. 22 when analyzed gives the reduced polygon of Fig. 23(b). This results in a phase-space sum:

$$\sum_{\vec{2},\vec{3}}\sum_{\vec{q}_1\vec{q}_2} N_2(\vec{q}_1\vec{q}_2) = N^2 \sum_{\vec{q}_1\vec{q}_2} N_2(\vec{q}_1\vec{q}_2)\ . \tag{3.23}$$

Within the statistical approximation [(3.13)–(3.16)] we obtain

$$N^2 \sum_{\vec{q}_1\vec{q}_2} N_2(\vec{q}_1\vec{q}_2) = \frac{1}{2^{3/2}}\, N^3Q^2 = QN^4\left(\frac{Q}{N}\right)\frac{1}{2^{3/2}}\ . \tag{3.24}$$

In Appendix B the techniques outlined above are used to calculate the weight factors for graphs of all orders composed of $n-1$ and $n-2$ cycles, i.e., the weights associated with $S_n^{(1)}$ and $S_n^{(2)}$. We find in general that the weight of an arbitrary graph of order n with $n-\alpha$ cycles can be written

$$QN^n(Q/N)^\alpha f[\hat{g}]\ , \tag{3.25}$$

where $f[\hat{g}]$ is a number associated with each graph such as 1 for the ladder diagrams or $(1/2)^{3/2}$ for the graph discussed above. It is the same number for large classes of graphs. (All of the ladder graphs have the same $f[\hat{g}]$ as do all of the graphs with $n-1$ cycles.) In the limit that $n\to\infty$, $f[\hat{g}]$ becomes a function only of α. In Sec. V we treat two limiting situations:

$$f[\hat{g}] = 1\ , \tag{3.26}$$

the Q/N model, and

$$f[\hat{g}] = f(\alpha)\ , \tag{3.27}$$

the $f(\alpha)$ model.

IV. ANALYSIS OF STRONGLY COUPLED BCS HAMILTONIAN

The topological identity of the graphs generated by the BCS and GBCS Hamiltonians makes it possible to write the expressions of interest in the GBCS case in terms of partial sums over related classes of BCS graphs. We can then obtain the spectra for the GBCS system by various analytic distortions of the BCS spectrum. To achieve this it is necessary to analyze carefully the strongly coupled BCS system; this we do now.

A. Diagramatic Analysis

Using the cycle-decomposition method, we found in Sec. III the following expression for the sum over all connected BCS diagrams of order n:

$$S_n = N^n\sum_{\alpha=0}^{n-2} S_n^{(\alpha)}(-1)^\alpha\left(\frac{1}{N}\right)^\alpha\ . \tag{4.1}$$

$S_n^{(\alpha)}$ is the number of graphs of the BCS topology of order n with $f = n-\alpha$ cycles; it is a positive number independent of N (the number of particles of one spin) or V (the magnitude of the coupling constant). As mentioned before, $S_n^{(0)}$, the number of ladder diagrams of order n, is easily seen to be $S_n^{(0)} = (n-1)!$ However, the numbers $S_n^{(1)}$, $S_n^{(2)}$, ... can only be found through a detailed study of the number of possible ways to form nth-order BCS diagrams consisting of $n-1$, $n-2$, ... cycles. In Appendix A we outline the calculation for $S_n^{(1)}$ and $S_n^{(2)}$. The results are

$$S_n^{(1)} = 2\binom{n}{3}(n-2)! = \frac{n-2}{3}\,n! \ , \tag{4.2}$$

$$\begin{aligned} S_n^{(2)} = &\left[4\binom{n}{4} + 48\binom{n}{5} + 96\binom{n}{6}\right](n-4)! \\ &+ \left[84\binom{n}{5} + 784\binom{n}{6} + 1680\binom{n}{7}\right. \\ &+ 2\binom{n}{3}\binom{n-3}{3} + 16\binom{n}{3}\binom{n-3}{4} \\ &\left. + \frac{80}{3}\binom{n}{4}\binom{n-4}{4}\right](n-5)! + 4\delta(n-4) \ . \end{aligned} \tag{4.3}$$

For $n = 4, 5, 6$, and 7 this formula must be interpreted with caution. For $n = 5$, for example, a term like

$$96\binom{n}{6}(n-4)!$$

does not contribute since this term, as shown in Appendix A, comes from the placements of a cycle covering six vertices, and there are only five vertices in a fifth-order graph. For $n \geq 8$ we find

$$S_n^{(2)} = n!\,(\tfrac{5}{108}\,n^3 - \tfrac{23}{90}\,n^2 + \tfrac{221}{540}\,n - \tfrac{8}{45}) \ . \tag{4.4}$$

For large values of n

$$\begin{aligned} S_n^{(0)} &= \frac{1}{n}\,n! \ , \\ S_n^{(1)} &\sim \frac{n}{3}\,n! \ , \\ S_n^{(2)} &\sim \frac{5n^3}{108}\,n! \ . \end{aligned} \tag{4.5}$$

For $\alpha \ll n$, the $S_n^{(\alpha)}$ appear to be an increasing sequence of numbers satisfying

$$S_n^{(\alpha+1)}/S_n^{(\alpha)} \gtrsim n^2 \ . \tag{4.6}$$

From these results we see that for any finite N the nonladder graphs will eventually dominate $S_n^{(0)}$. The sequence

$$S_n = N^n \sum_{\alpha=0}^{n-2} S_n^{(\alpha)} \left(-\frac{1}{N}\right)^{\alpha}$$

is therefore dominated by $S_n^{(0)}$ only as long as

$$n \lesssim (3N)^{1/2} \ . \tag{4.7}$$

Beyond this, all of the terms of (4.1) contribute. Since the terms oscillate in sign, the sum depends rather delicately on the magnitude of all of the terms. From this the effect of the exclusion principle is clearly visible. No matter how large N is, if one goes to sufficiently high order $[n \gtrsim (3N)^{1/2}]$ the exclusion of phase space due to the Pauli principle becomes of dominating importance.

The subsequences

$$\sum_{n=1}^{\infty} S_n^{(\alpha)} \frac{y^n}{n!} \equiv B^{(\alpha)}(y) \tag{4.8}$$

can easily be summed when $S_n^{(\alpha)}$ are known. For $\alpha = 1$

$$B^{(1)}(y) = \sum_{n=3}^{\infty} \left(\frac{n-2}{3}\right) y^n = \frac{1}{3}\,\frac{y^3}{(1-y)^2} \ ,$$

and for $\alpha = 2$ $B^{(2)}(y)$ contains terms of the form

$$\frac{y^s}{(1-y)^{s+1}} + \text{polynomials in } y.$$

Each of these nonpolynomial terms and (as has been shown previously) also $B^{(0)}(y)$ has a singularity at $y = 1$. For $\alpha = 1$ and 2, however, the singularities are poles. We conjecture that for all $\alpha > 0$, $B^{(\alpha)}(y)$ has a pole of some order at $y = 1$. In the sum over α, however, it is very likely that this pole is displaced.

B. Exact Solution

The energy spectrum and degeneracies for the strongly coupled BCS Hamiltonian have been calculated by Anderson[3] and by Thouless.[4] They find the following:

$$E_r = -V[N^2 + N - r(2N - r + 1)] \ , \tag{4.9}$$

$$d_r = \frac{(2N)!\,(2N - 2r + 1)}{r!\,(2N - r + 1)!} \ , \tag{4.10}$$

where E_r is the energy of the rth level and d_r is the number of degenerate levels at that energy. The lowest level of this system is

$$E_0 = -VN(N+1) \tag{4.11}$$

and is nondegenerate while the highest level is

$$E_N = 0 \tag{4.12}$$

and is $(N+1)^{-1}[(2N)!/(N!)^2]$-fold degenerate. This is a spectrum characteristic of a classic superconductor: a nondegenerate vacuum, the first excited states removed from the vacuum by the energy gap

$$2\Delta = 2NV \ , \tag{4.13}$$

and the higher excited states becoming more and more degenerate until the highest level which has a degeneracy equal to $(N+1)^{-1} \times$(the total number of states). The spectrum is shown in Fig. 24.

The total number of states of this system is

$$\sum_{r=0}^{N} d_r = \frac{(2N)!}{(N!)^2} \ , \tag{4.14}$$

which is the number of states counting only the "pair" excitations—the excitations of the system which correspond to configurations of the noninteracting system in which single-particle states are occupied in pairs (if $\vec{k}\uparrow$ is occupied, $-\vec{k}\downarrow$ is occupied also). The total number of configurations

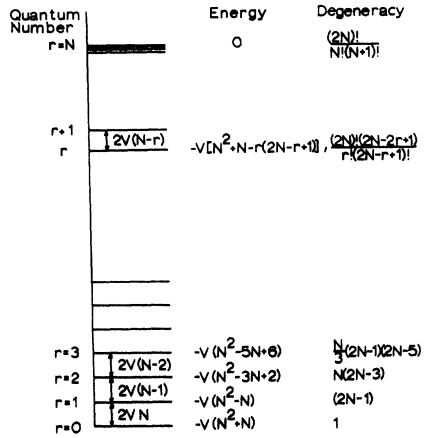

FIG. 24. Energy spectrum for H_{BCS} in the strong-coupling limit.

which result is that of N particles in $2N$ available states. This is just

$$(2N)!/(N!)^2 .$$

"Single-particle" excitations are included in this spectrum in a completely passive way. Since the Hamiltonian connects only "pair" states, any single particles do nothing further than occupy phase space and so reduce the number of possible transitions of the pairs.

If q is the number of single-particle excitations, the number of pair states available is reduced to

$$2N - q,$$

while the number of pairs is reduced to

$$N - \tfrac{1}{2}q .$$

The energy of such excited states is

$$E_r = -V[(N - \tfrac{1}{2}q)(N - \tfrac{1}{2}q + 1) - r(2N - q - r + 1)] .$$

The lowest energy of the state with two excited single particles ($q = 2$, $r = 0$) is $-NV(N-1)$ which is just the energy of the state with no single-particle excitations and one excited pair ($q = 0$, $r = 1$). This is analogous to the energies of pair and single excitations in the BCS theory.

Using the results of Sec. II and (4.1), we have

$$\exp\left[\sum_{n\alpha} S_n^{(\alpha)} (-1)^\alpha \left(\frac{1}{N}\right)^\alpha \frac{(NVt)^n}{n!}\right]$$

$$= \langle \phi_0 | e^{-H_{BCS} t} | \phi_0 \rangle$$

$$= \sum_m |\langle \phi_0 | \psi_m \rangle|^2 e^{-E_m t} , \qquad (4.15)$$

where $|\phi_0\rangle$ is the unperturbed vacuum defined preceding (2.10) and H_{BCS} above is the BCS strongly coupled Hamiltonian (2.13). The eigenstates of H_{BCS} are $|\psi_m\rangle$, and E_m are the corresponding eigenvalues.

Introducing

$$y = NVt , \qquad (4.16)$$

$$\epsilon_m = -E_m/NV , \qquad (4.17)$$

we have

$$\exp\left[\sum_{n\alpha} S_n^{(\alpha)} (-1)^\alpha \left(\frac{1}{N}\right)^\alpha \frac{y^n}{n!}\right] = \sum_m |\langle \phi_0 | \psi_m \rangle|^2 e^{y\epsilon_m} , \qquad (4.18)$$

where ϵ_m is seen from Eq. (4.9) to be a positive number ranging from 0 to $N+1$.

In Sec. III C it was shown that S_n is independent of the unperturbed state $|\phi_i\rangle$ used as a vacuum. We can from this conclude that

$$|\langle \phi_0 | \psi_m \rangle|^2 = \text{const} = \frac{1}{\text{number of states}} = \frac{(N!)^2}{(2N)!} . \qquad (4.19)$$

We therefore rewrite the sum on the right-hand side of (4.18) as

$$\sum_{r=0}^{N} \mathcal{d}_r e^{y\epsilon_r} , \qquad (4.20)$$

where

$$\mathcal{d}_r = \frac{\text{degeneracy of the } r\text{th level}}{\text{total number of levels}} = \frac{(N!)^2}{(2N)!} d_r = \frac{(N!)^2 (2N - 2r + 1)}{r!\,(2N - r + 1)!} . \qquad (4.21)$$

From this it follows that

$$\sum_{r=0}^{N} \mathcal{d}_r = 1 . \qquad (4.22)$$

This implies that

$$S_0^{(0)} \equiv S_0 = 0 . \qquad (4.23)$$

Since further

$$\frac{\partial}{\partial y} \sum_{r=0}^{N} \mathcal{d}_r e^{y\epsilon_r} \bigg|_{y=0} = \sum_{r=0}^{N} \mathcal{d}_r \epsilon_r = -\frac{1}{NV}\left(\frac{1}{\text{no. of states}}\right)(\text{trace}) = 1 , \qquad (4.24)$$

we have

$$S_1 = S_1^{(0)} = 1 . \qquad (4.25)$$

It is convenient to define

$$G(N, y) \equiv \sum_{r=0}^{N} \mathcal{d}_r e^{y\epsilon_r} , \qquad (4.26)$$

$$\mathcal{G}(N, y) \equiv \ln G(N, y) . \qquad (4.27)$$

We then can write

$$\sum_{n\alpha} S_n^{(\alpha)} (-1)^\alpha \left(\frac{1}{N}\right)^\alpha \frac{y^n}{n!} = \mathcal{G}(N, y) . \qquad (4.28)$$

Using the known expressions (4.9) and (4.10) for E_r and d_r, respectively, both G and $\mathcal{G}$ are known functions of y and N. The series on the left-hand side of (4.28) has a nonzero radius of convergence in y. $S_n^{(\alpha)}$ can be calculated from H_{BCS} by the methods of Appendix A.

V. ANALYSIS OF GBCS HAMILTONIAN

A. $f(\alpha)$ Model

For the GBCS Hamiltonian the most general weight of a connected graph of order n with $n-\alpha$ cycles is

$$QN^n (Q/N)^\alpha f[\hat{g}] \ . \tag{5.1}$$

The functional $f[\hat{g}]$, where $\hat{g}$ refers to a particular graph, can be calculated using the methods of Sec. III and Appendix B. In Appendix B, $f[\hat{g}]$ is calculated explicitly for all graphs for which $\alpha = 1$ and $\alpha = 2$. It is found for these values of α that in the $n \to \infty$ limit $f[\hat{g}]$ depends only on α, and it can be seen that this is the case for all values of α for large enough n. This leads us to define what we call the $f(\alpha)$ model—where $f[\hat{g}]$ is a function only of α:

$$f[\hat{g}] = f(\alpha) \ .$$

In this model the contribution of the sum of all graphs of order n composed of $n-\alpha$ cycles is

$$QN^n S_n^{(\alpha)} (-1)^\alpha (Q/N)^\alpha f(\alpha) \ , \tag{5.2}$$

so that

$$\ln(\langle\phi_0| e^{-Ht} |\phi_0\rangle) = \ln(\textstyle\sum_m |\langle\phi_0|\psi_m\rangle|^2 e^{-E_m t}) = Q\sum_n S_n^\alpha (-1)^\alpha \left(\frac{Q}{N}\right)^\alpha f(\alpha) \frac{(NVt)^n}{n!} \ . \tag{5.3}$$

This can be generated from the analogous expression for the BCS case by first making the substitutions

$$N \to (N/Q) e^{p} \ , \quad V \to (VQ) e^{-p} \tag{5.4}$$

in (4.28):

$$\mathcal{G}(N, y) = \ln G(N, y) = \sum_{n\alpha} S_n^{(\alpha)} (-1)^\alpha \left(\frac{1}{N}\right)^\alpha \frac{y^n}{n!} \ .$$

If we multiply this with $Qg(p)$ where $g(p)$ is defined by

$$f(\alpha) = \int_0^\infty g(p) e^{-\alpha p} dp \tag{5.5}$$

and integrate, we obtain for the right-hand side

$$Q\int_0^\infty g(p) dp \sum_{n\alpha} S_n^{(\alpha)} (-1)^\alpha \left(\frac{Q}{N}\right)^\alpha e^{-\alpha p} \frac{y^n}{n!} \ . \tag{5.6}$$

Interchanging the summation and integration yields

$$Q\sum_{n\alpha} S_n^{(\alpha)} (-1)^\alpha \left(\frac{Q}{N}\right)^\alpha f(\alpha) \frac{y^n}{n!} \ . \tag{5.7}$$

All of the operations are valid if $g(p)$ is compact, $g(p) = 0$ for $p > p_{\max}$. In that case $0 < N - (N/Q) e^{p} < \infty$ and the sequence (5.6) is absolutely convergent. The justification for these operations will be given elsewhere where we discuss the analytic properties of G and $\mathcal{G}$. From (4.26) and (4.27) we have

$$\mathcal{G}(N, y) = \ln\left(\sum_{r=0}^{N} \vec{d}_r e^{y\epsilon_r(N)}\right) \ ,$$

and we may now write

$$\ln(\textstyle\sum_m |\langle\phi_0|\psi_m\rangle|^2 e^{y\epsilon_m}) = Q \int_0^\infty g(p) dp \ \mathcal{G}(Ne^{p}/Q, y) \ . \tag{5.8}$$

[In this section E_m and ϵ_m refer to the energy levels of the GBCS system ($\epsilon_m = -E_m/NV$). To distinguish these from the corresponding energy levels of the BCS system, we write the latter in this section always as $\epsilon_m(N)$ or $\epsilon_m(Ne^{p}/Q)$.] To evaluate this we consider the asymptotic limit $y \to \infty$. In this limit the function G is dominated by

$$\lim_{y\to\infty} \left(\sum_{r=0}^{N} \vec{d}_r \, e^{y\epsilon_r}\right) \to \vec{d}_0 e^{y\epsilon_0} \ , \tag{5.9}$$

so that

$$\lim_{y\to\infty} \mathcal{G}(N, y) = \ln \vec{d}_0(N) + y\,\epsilon_0(N) \ .$$

To identify the various levels we write

$$\mathcal{G}(N, y) = \ln \vec{d}_0(N) + y\epsilon_0(N) + \ln\left(1 + \sum_{r=1}^{N} d_r(N) e^{y\Delta_r(N)}\right) \ , \tag{5.10}$$

where d_r is the degeneracy of the rth level,

$$d_r(N) = \frac{\vec{d}_r(N)}{\vec{d}_0(N)} = \frac{(2N)!\,(2N-2r+1)}{r!\,(2N-r+1)!} \ ,$$

and

$$\Delta_r(N) = \epsilon_r(N) - \epsilon_0(N) = -2r + (r/N)(r-1) \ . \tag{5.11}$$

We therefore obtain

$$\ln(|\langle\phi_0|\psi_0\rangle|^2) + y\epsilon_0 + \ln\left(\sum_m \frac{|\langle\phi_0|\psi_m\rangle|^2}{|\langle\phi_0|\psi_0\rangle|^2} e^{y\delta_m}\right) = Q\int_0^\infty dp\, g(p) \left\{ \ln \vec{d}_0\left(\frac{Ne^{p}}{Q}\right) + y\epsilon_0\left(\frac{Ne^{p}}{Q}\right) + \ln\left[1 + \sum_{r=1}^{N} d_r \left(\frac{Ne^{p}}{Q}\right) e^{y\Delta_r(Ne^{p}/Q)}\right]\right\} \ , \tag{5.12}$$

where

$$\delta_m = \epsilon_m - \epsilon_0 \ . \tag{5.13}$$

In the $y \to \infty$ limit the first two terms give

$$\ln(|\langle\phi_0|\psi_0\rangle|^2) = Q\int_0^\infty dp\, g(p) \ln \vec{d}_0(Ne^{p}/Q) \tag{5.14}$$

and

$$y\epsilon_0 = Q\int_0^\infty dp\, g(p) [y\,(N/Q) e^{p} + y] = y\,[Nf(-1) + Qf(0)] \ . \tag{5.15}$$

Since $f(0) \equiv 1$ from the normalization of the ladder graphs, we have for the ground state of the GBCS system in the $f(\alpha)$ approximation

$$\epsilon_0 = Nf(-1) + Q \tag{5.16}$$

or

$$E_0 = -VN^2[f(-1) + (Q/N)] \ . \tag{5.17}$$

We now recall that

$$\vec{a}_0(N) = (N!)^2/(2N)! \ .$$

Evaluated by Stirling's formula in the limit of large N this yields

$$\vec{a}_0(N) \sim (\pi N)^{1/2} \ (\tfrac{1}{2})^{2N} \ . \tag{5.18}$$

We therefore have

$$\ln \vec{a}_0 (Ne^{p}/Q) = \tfrac{1}{2} \ln(\pi N/Q) + \tfrac{1}{2} p - (2N/Q) e^{p} \ln 2 \ . \tag{5.19}$$

Substituted into (5.14) this yields

$$\ln |\langle \phi_0 | \psi_0 \rangle|^2 = Q \int_0^\infty dp \, g(p) \ln \vec{a}_0(Ne^{p}/Q)$$

$$= \tfrac{1}{2} Qf(0) \ln(\pi N/Q) - \tfrac{1}{2} Qf'(0) - 2Nf(-1) \ln 2 \ . \tag{5.20}$$

Since $f(0) = 1$ we have

$$\ln |\langle \phi_0 | \psi_0 \rangle|^2 = \tfrac{1}{2} Q \ln(\pi N/Q) - \tfrac{1}{2} Qf'(0) - 2Nf(-1) \ln 2 \ . \tag{5.21}$$

From this it follows that

$$f(-1) = \frac{Q}{4N \ln 2} \left(\ln \frac{\pi N}{Q} - f'(0) \right) - \frac{1}{2N \ln 2} \ln |\langle \phi_0 | \psi_0 \rangle|^2 \ . \tag{5.22}$$

In the asymptotic ($y \to \infty$) limit the other energy levels can be separated and identified. The expression of interest is

$$\int_0^\infty g(p) \ln(1 + d_1 e^{y\Delta_1} + d_2 e^{y\Delta_2} + \cdots)^Q dp \ . \tag{5.23}$$

The first few terms are

$$(1 + d_1 e^{y\Delta_1} + \cdots)^Q = 1 + Q d_1 e^{y\Delta_1} + \frac{Q(Q-1)}{2!} d_1^2 e^{2y\Delta_1} + Q d_2 e^{y\Delta_2}$$

$$+ \frac{Q(Q-1)(Q-2)}{3!} d_1^3 e^{3y\Delta_1} + \frac{Q(Q-1)}{2!} d_1 d_2 e^{y(\Delta_1 + \Delta_2)} + Q d_3 e^{y\Delta_3} + \cdots \ . \tag{5.24}$$

Since $Q/N \ll 1$ we have approximately

$$d_1 \simeq (2N/Q) e^{p} \ , \quad d_2 \simeq 2(N/Q)^2 e^{2p} \ , \quad d_3 \simeq \tfrac{4}{3} (N/Q)^3 e^{3p} \ . \tag{5.25}$$

This gives

$$(1 + d_1 e^{y\Delta_1} + \cdots)^Q \simeq 1 + 2Ne^{p} e^{-2y} + 2N^2 e^{2p} e^{-4y} + 2N(N/Q) e^{2p} e^{-4y} e^{-2y(Q/N)e^{-p}}$$

$$+ \tfrac{4}{3} N^3 e^{3p} e^{-6y} + 2N^2 (N/Q) e^{3p} e^{-6y + y(2Q/N)e^{-p}} + \tfrac{4}{3} N (N/Q)^2 e^{3p} e^{-6y + y(6Q/N)e^{-p}} + \cdots \ . \tag{5.26}$$

Therefore

$$\int_0^\infty g(p) dp \ln(1 + 2Ne^{p} e^{-2y} + \cdots) = \ln \left(\sum_m \frac{|\langle \phi_0 | \psi_m \rangle|^2}{|\langle \phi_0 | \psi_0 \rangle|^2} \ e^{y\delta_m} \right) \equiv \ln(1 + \textstyle\sum_1 a_1 e^{y\delta_1} + \sum_2 a_2 e^{y\delta_2} + \cdots) \ , \tag{5.27}$$

where by $\sum_i a_i e^{y\delta_i}$ we imply a sum over the states clustered about the ith level. Expanding a logarithm of the form

$$\ln(1 + x_1 + x_2 + x_3 + \cdots) \ ,$$

where $x_i x_j$ is of order x_k if $i + j = k$, and sorting out powers, we obtain

$$\ln(1 + x_1 + x_2 + x_3 + \cdots) = x_1 + x_2 - \tfrac{1}{2} x_1^2 + x_3 - \tfrac{1}{2} 2x_1 x_2 + \tfrac{1}{3} x_1^3 + \cdots \ . \tag{5.28}$$

Now expanding the logarithm in the integral on the left-hand side of (5.27) we have

$$\int_0^\infty g(p) dp \{ e^{p} e^{-2y} 2N + e^{2p} e^{-4y} [2N^2 + 2N(N/Q) e^{2y(Q/N)e^{-p}} - \tfrac{1}{2} 4N^2]$$

$$+ e^{3p} e^{-6y} [\tfrac{4}{3} N^3 + 2N^2 (N/Q) e^{2y(Q/N)e^{-p}} + \tfrac{4}{3} N (N/Q)^2 e^{6y(Q/N)e^{-p}}$$

$$- 4N^3 - 4N^2 (N/Q) e^{2y(Q/N)e^{-p}} + \tfrac{1}{3} 8N^3] + O(e^{-8y}) \cdots \} \ . \tag{5.29}$$

With integration and cancellation of terms this gives

$$e^{-2y}\,2Nf(-1)+e^{-4y}\,2N(N/Q)F_{22}(y)$$
$$+e^{-6y}\left[\tfrac{4}{3}N(N/Q)^2F_{36}(y)-2N^2(N/Q)F_{32}(y)\right]+\text{higher-order terms}, \tag{5.30}$$

where we have defined

$$F_{rs}(y)\equiv\int_0^\infty g(p)\,e^{rp}e^{ys(Q/N)e^{-p}}dp\ . \tag{5.31}$$

All of this is equal to the right-hand side of (5.27) which when expanded gives

$$\ln(1+\textstyle\sum_1 a_1e^{y\delta_1}+\sum_2 a_2e^{y\delta_2}+\cdots)=\sum_1 a_1e^{y\delta_1}+\sum_2 a_2e^{y\delta_2}-\tfrac{1}{2}(\sum_1 a_1e^{y\delta_1})^2$$
$$+\textstyle\sum_3 a_3e^{y\delta_3}-\sum_1\sum_2 a_1a_2e^{y(\delta_1+\delta_2)}+\tfrac{1}{3}(\sum_1 a_1e^{y\delta_1})^3+\text{higher-order terms}. \tag{5.32}$$

Equating the various orders, we have

$$\textstyle\sum_1 a_1e^{y\delta_1}=e^{-2y}\,2Nf(-1)\ , \tag{5.33}$$

so that

$$\textstyle\sum_1 a_1=2Nf(-1)\ \text{ and }\ \delta_1=-2\ , \tag{5.34}$$

$$\textstyle\sum_2 a_2e^{y\delta_2}=\{2N(N/Q)F_{22}(y)+\tfrac{1}{2}(4N^2)[f(-1)]^2\}e^{-4y}\ , \tag{5.35}$$

$$\textstyle\sum_3 a_3e^{y\delta_3}=e^{-6y}\{4N^2(N/Q)f(-1)F_{22}(y)+4N^3[f(-1)]^3-\tfrac{1}{3}8N^3[f(-1)]^3+\tfrac{4}{3}N(N/Q)^2F_{36}(y)-2N^2(N/Q)F_{32}(y)\}$$
$$=e^{-6y}\{\tfrac{4}{3}N^3[f(-1)]^3+4N^2(N/Q)[f(-1)F_{22}-\tfrac{1}{2}F_{32}]+\tfrac{4}{3}N(N/Q)^2F_{36}(y)\}\ . \tag{5.36}$$

The ground state for the $f(\alpha)$ model is given by (5.17). The first grouping of excited states is obtained from

$$\textstyle\sum_1 a_1e^{y\delta_1}=2Nf(-1)e^{-2y}\ ,$$

so that we have a level at

$$E_1=E_0+2NV, \tag{5.37}$$

with a relative weight of

$$\textstyle\sum_1\frac{|\langle\phi_0|\psi_1\rangle|^2}{|\langle\phi_0|\psi_0\rangle|^2}=2Nf(-1)\ . \tag{5.38}$$

We see, therefore, that there is a gap in the energy spectrum of $2NV$ between the ground state and the first excited states.

The higher groupings of states are spread about a dominant level by the function

$$F_{rs}(y)=\int_0^\infty g(p)\,e^{rp}e^{ys(Q/N)e^{-p}}dp\ , \tag{5.39}$$

where

$$0\leq s(Q/N)e^{-p}\leq s\,Q/N\ . \tag{5.40}$$

We recall that

$$f(\alpha)=\int_0^\infty g(p)\,e^{-p\alpha}dp$$

and that

$$f(0)=\int_0^\infty g(p)\,dp=1\ .$$

The function $F_{rs}(y)$ may be regarded as spreading states originally degenerate by the amount sVQ. Consider, for example,

$$\textstyle\sum_2 a_2e^{y\delta_2}=\sum_2\frac{|\langle\phi_0|\psi_2\rangle|^2}{|\langle\phi_0|\psi_0\rangle|^2}\,e^{(\epsilon_2-\epsilon_0)}$$
$$=\{2N(N/Q)F_{22}(y)+\tfrac{1}{2}(4N^2)[f(-1)]^2\}e^{-4y}\ . \tag{5.41}$$

The highest level of this group is given by

$$(\epsilon_2-\epsilon_0)y=-4y\ ,$$

and recalling that $y=NVt$ and $\epsilon_m=-E_m/NV$, we have

$$E_2^{\text{highest}}-E_0=4NV\ . \tag{5.42}$$

Therefore, the highest level of this second grouping of states is removed from the ground state by $4NV$. The lowest level of this grouping is

$$E_2^{\text{lowest}}-E_0=4NV-2VQ\ . \tag{5.43}$$

Thus, this second grouping of levels is spread between

$$E_0+4NV\ \text{ and }\ E_0+4NV(1-\tfrac{1}{2}Q/N)\ .$$

As long as $Q/N\ll 1$, this group of levels is separated from the lowest excited states by an energy of about $2NV$.

In a similar manner one finds the third grouping of levels spread between

$$E_0+6NV\ \text{ and }\ E_0+6NV(1-Q/N)\ .$$

The lowest part of the spectrum is shown in Fig. 25.

B. Q/N Model

One interesting limit occurs if we set $f[\hat{g}]$

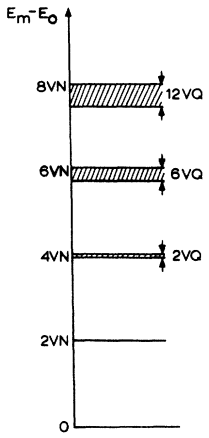

FIG. 25. Lowest part of the energy spectrum for the $f(\alpha)$ model.

$= f(\alpha) = 1$ as in (3.26). This is equivalent to letting

$$N_s(\vec{q}_1 \ldots \vec{q}_s) = N \text{ for } |\vec{q}_1| \ldots |\vec{q}_s| \leq q_0$$
$$= 0 \text{ elsewhere.} \quad (5.44)$$

In doing this we take no account of the reduction in weight produced by the higher-order polygons. This is the simplest approximation we make in summing the graphs generated by H_{GBCS}; each electron $-\vec{i}\downarrow$ interacts equally with all of the electrons in the sphere with Q states of spin $\uparrow$ centered about $\vec{i}$ in such a way that the weight contributed by one $s+1$ point polygon (or a cycle of order $s+1$) is just NQ^s. We call the model so defined the Q/N model.

It has previously been shown that a BCS ladder graph of order n has the weight N^n. An nth-order BCS graph containing $n-\alpha$ cycles (where α is no larger than $n-2$) has the weight

$$N^n(1/N)^\alpha \ .$$

In a similar fashion for the Q/N model, a ladder graph of the nth order has the weight

$$QN^n \ , \quad (5.45)$$

while the nth-order graph containing $n-\alpha$ cycles has the weight

$$QN^n(Q/N)^\alpha \ . \quad (5.46)$$

This leads to an expression for the sum over connected graphs of order n for the Q/N model:

$$S_n = QN^n\left[S_n^{(0)} - \left(\frac{Q}{N}\right)S_n^{(1)} + \left(\frac{Q}{N}\right)^2 S_n^{(2)} + \cdots \left(-\frac{Q}{N}\right)^{n-2} S_n^{(n-2)}\right], \quad (5.47)$$

compared with the BCS expression

$$S_n^{\mathrm{BCS}} = N^n\left[S_n^{(0)} - \left(\frac{1}{N}\right)S_n^{(1)} + \left(\frac{1}{N}\right)^2 S_n^{(2)} + \cdots \left(-\frac{1}{N}\right)^{n-2} S_n^{(n-2)}\right]. \quad (5.48)$$

Putting these into (2.23) and (2.24), we obtain for the vacuum expectation value of the U matrix for the two cases

$$\langle U(-it)\rangle_0 = \exp\left[\sum_{\alpha=0}^{\infty}\left(-\frac{1}{N}\right)^\alpha B_0^{(\alpha)}(NVt)\right], \text{ BCS} \quad (5.49)$$

$$= \exp\left[Q\sum_{\alpha=0}^{\infty}\left(-\frac{Q}{N}\right)^\alpha B_0^{(\alpha)}(NVt)\right], \text{ GBCS} \quad (5.50)$$

where

$$B_0^{(\alpha)}(NVt) = \sum_{n=1}^{\infty}\frac{S_n^{(\alpha)}}{n!}(NVt)^n \quad (5.51)$$

and

$$S_n^{(\alpha)} = 0 \text{ for } \alpha > n-2 \ .$$

The sequence can now be obtained from the reference strongly coupled BCS sequence by making the substitution

$$N \to N/Q \ , \quad V \to VQ \ , \quad (5.52)$$

and multiplying the series by Q. Since Q is a positive number larger than 1 ($Q=1$ is the BCS case), the transformation leaves NV and therefore $y = NVt$ unaltered and maps the real line (excluding 0 and ∞) into itself. Hence the energy spectrum for the Q/N model can be expressed in terms of the spectrum for the strongly coupled BCS Hamiltonian. We may also obtain the spectrum by setting $f(\alpha) = 1$ in Sec. V A.

We find

$$\sum_m |\langle\phi_0|\psi_m\rangle|^2 e^{y\epsilon_m} = [\sum_r \vec{a}_r (N/Q)\, e^{y\epsilon_r(N/Q)}]^Q \ , \quad (5.53)$$

where as before

$$\epsilon_r(N) = N + 1 - 2r + (r/N)(r-1). \quad (5.54)$$

The matrix element $|\langle\phi_0|\psi_m\rangle|^2$, by an argument similar to that in Sec. IV, will be proportional to the degeneracy of the mth level of the exact system; therefore both the energy levels and the degenerate structure can be evaluated from (5.53).

With the methods described above we obtain for the ground-state energy of the Q/N model

$$E_0 = -N^2V(1 + Q/N) \ . \quad (5.55)$$

[This is to be compared with the ground-state energy in the strongly coupled BCS model of $-N^2V(1+1/N).$]

The lowest energy levels are given by following expression:

$$E_m = E_0 + 2VN(l_0 + l_1 + l_2 + l_3 + \cdots) - 2VQ(l_1 + 2l_2 + 3l_3 + \cdots) \ , \quad (5.56)$$

where l_0, l_1, l_2... are integers which satisfy

$$l_0 \geq l_1 \geq l_2 \geq l_3 > \cdots \ . \tag{5.57}$$

There is a first grouping of excited levels at

$$E_1 = E_0 + 2NV, \tag{5.58}$$

with the weight

$$2N(1 - Q/2N) \ , \tag{5.59}$$

and a second grouping of excited levels at

$$E_2^{\text{lowest}} = E_0 + 4NV(1 - \tfrac{1}{2}Q/N), \tag{5.60}$$

with the weight

$$2N(N/Q)(1 - \tfrac{3}{2}Q/N) \ , \tag{5.61}$$

and

$$E_2^{\text{highest}} = E_0 + 4NV, \tag{5.62}$$

with the weight

$$(4N^2 - 4NQ + Q^2)(1 - 1/Q) \ . \tag{5.63}$$

The Q/N spectrum is thus spaced in discrete units over the region of spread in the $f(\alpha)$ model. The lowest part of the spectrum is shown in Fig. 26.

In the limit of $Q = 1$, the GBCS model in the Q/N approximation gives, as expected, the BCS result. For

$$1/N \ll Q/N \ll 1 \ ,$$

one would expect that the ladder and lower-order diagrams would be underestimated; a more accurate estimate of the contributions of higher-order diagrams should take into account the reduction in the higher-order graphs due to the reduced contribution of the polygon functions $N_s(\tilde{q}_1 \ldots \tilde{q}_s)$. This is accomplished in the $f(\alpha)$ model described previously.

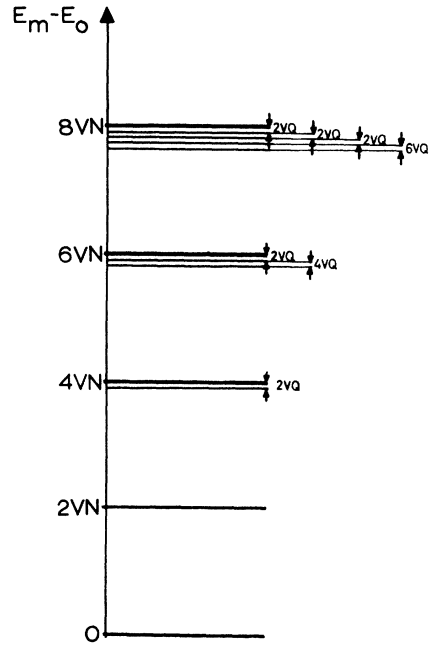

FIG. 26. Lowest part of the energy spectrum for the Q/N model.

C. Estimate of $f(-1)$

The function $f(\alpha)$ decreases monotonically with increasing α and $f(0) = 1$. The analytic continuation of $f(\alpha)$ onto the negative real axis gives both the ground state, excited states, and degeneracies for the $f(\alpha)$ model. In particular $f(-1)$ determines the ground-state energy. Since $f(\alpha)$, in principle, can be calculated for all positive integral values of α, $f(\alpha)$ is determined; we need the analytic continuation of $f(\alpha)$ into the left half-plane. This will always be possible since

$$f(\alpha) = \int_0^\infty g(p)\, e^{-\alpha p} dp, \tag{5.64}$$

with $g(p) = 0$ for $p > p_{\max}$ in order that $Ne^p/Q < \infty$.

In absence of a complete knowledge of $f(\alpha)$, bounds on $f(-1)$ can be obtained using a type of sum rule with a limited number of assumptions in the following way. We have previously obtained

$$f(-1) = \frac{Q}{4N \ln 2}\left(\ln\frac{\pi N}{Q} - f'(0)\right) - \frac{1}{2N \ln 2} \ln |\langle \phi_0 | \psi_0 \rangle|^2$$

(where it is assumed that the ground state of the interacting system is nondegenerate).

The ground state of the GBCS Hamiltonian can be expanded in states of the "unperturbed" system as

$$|\psi_0\rangle = \sum_m |\phi_m\rangle\langle\phi_m|\psi_0\rangle \ , \tag{5.65}$$

where the sum goes over all states connected to the "unperturbed" vacuum by the vertices of the GBCS Hamiltonian. This guarantees that all the states $|\phi_m\rangle$ for which $\langle\phi_m|\psi_0\rangle \neq 0$ have zero total momentum as well as equal numbers of particles and holes of up and down spin:

$$\langle\phi_m|p_\uparrow^* p_\uparrow|\phi_m\rangle = \langle\phi_m|p_\downarrow^* p_\downarrow|\phi_m\rangle = \langle\phi_m|h_\uparrow^* h_\uparrow|\phi_m\rangle$$
$$= \langle\phi_m|h_\downarrow^* h_\downarrow|\phi_m\rangle \ . \tag{5.66}$$

For the strongly coupled BCS Hamiltonian, any eigenstate state $|\psi_i\rangle$ is a sum over all of the pair states, each term having equal weight; only the phase varies:

$$|\psi_i\rangle = \left(\frac{1}{\text{number of pair states}}\right)^{1/2} \sum_j e^{i\gamma_{ij}} |\phi_j\rangle \ .$$

For the ground state, $\gamma_{ij} = 0$, so that

$$|\langle\phi_0|\psi_0\rangle|^2 = \frac{1}{\text{number of pair states}} = \frac{(N!)^2}{(2N)!} \ . \tag{5.67}$$

For the ground state of the GBCS Hamiltonian we write

$$|\psi_0\rangle = \sum_{\text{BCS pair states}} \alpha_i |\phi_i\rangle + \sum_{\text{other states}} \beta_i |\phi_i\rangle \ , \tag{5.68}$$

where presumably in analogy with (5.67) the α_i are equal and $|\beta_i| < |\alpha_i|$. We then have

$$\langle\phi_0|\psi_0\rangle = \alpha_0$$

(the component of the "unperturbed" vacuum in the ground state of GBCS).

To obtain a lower bound for $f(-1)$ we want the largest possible value of $|\alpha_0|$. We obtain this if we couple $|\psi_0\rangle$ *only* to the BCS-type pair states. We know (from the variational nature of the BCS ground state) that $|\psi_0\rangle$ must be coupled equally to $|\phi_0\rangle$ and to all other BCS-type pair states $|\phi_i\rangle$. From this we can conclude that if the $\beta_i = 0$ (thus that $|\psi_0\rangle$ is just the BCS ground state),

$$\langle\phi_0|\psi_0\rangle = \alpha_0 = \left(\frac{1}{\text{number of BCS pair states}}\right)^{1/2} = \left(\frac{(N!)^2}{(2N)!}\right)^{1/2} \ . \tag{5.69}$$

It then follows, using Stirling's formula, that

$$\ln|\alpha_0|^2 = \ln\frac{(N!)^2}{(2N)!} \sim \tfrac{1}{2}\ln\pi N - 2N\ln 2 \ , \tag{5.70}$$

so that

$$f(-1) \geq \frac{Q}{4N\ln 2}\left(\ln\frac{\pi N}{Q} - f'(0)\right) - \frac{\ln\pi N}{4N\ln 2} + 1 \ . \tag{5.71}$$

Since $f'(0)$ is not large compared with $\ln(\pi N/Q)$ [we can determine this by inspection since $f(0) = 1$ and we are able to calculate $f(1)$, $f(2)$, etc.] and $\ln\pi N \ll Q$, we have

$$f(-1) \gtrsim 1 + \frac{Q}{4N\ln 2}\ln\frac{\pi N}{Q} \ . \tag{5.72}$$

To find an upper bound for $f(-1)$ we need the minimum value of $\ln|\langle\phi_0|\psi_0\rangle|^2$. This we obtain if we let $|\psi_0\rangle$ be constructed from an equal weighting of all the states to which $|\psi_0\rangle$ is connected by the vertices of the GBCS Hamiltonian. From (5.68)

$$\langle\psi_0|\psi_0\rangle = 1 = \sum_{\substack{\text{BCS pair}\\ \text{states}}} |\alpha_i|^2 + \sum_{\substack{\text{other}\\ \text{states}}} |\beta_i|^2 \ .$$

If all the $|\alpha_i|$ and $|\beta_i|$ are equal, we have

$$|\alpha_0|^2 = 1/C \ , \tag{5.73}$$

where C is the total number of configurations which are connected to $|\psi_0\rangle$ by the vertices of the GBCS Hamiltonian and which have zero total momentum. But this last expression is larger than that obtained if we assume that *all* of the GBCS configurations even those not satisfying (5.66) or whose momentum is not equal to zero are connected equally with $|\psi_0\rangle$. The total number of GBCS configurations is

$$[(2N)!/(N!)^2]^2 \ ,$$

so that if $|\alpha_i| = |\beta_i| = \text{const}$, we have

$$|\alpha_0|^2 \geq [(N!)^2/(2N)!]^2 \ ,$$

$$\ln|\alpha_0|^2 = \ln|\langle\phi_0|\psi_0\rangle|^2 \gtrsim \ln\pi N - 4N\ln 2 \ ,$$

so that

$$f(-1) \lesssim 2 + \frac{Q}{4N\ln 2}\ln\frac{\pi N}{Q} \ . \tag{5.74}$$

Therefore, we can reasonably bound $f(-1)$ by

$$1 + \frac{Q}{4N\ln 2}\ln\frac{\pi N}{Q} \lesssim f(-1) \lesssim 2 + \frac{Q}{4N\ln 2}\ln\frac{\pi N}{Q} \ . \tag{5.75}$$

Another method by which we might estimate $f(-1)$ is to consider the matrix element

$$\sum_1 \frac{|\langle\phi_0|\psi_1\rangle|^2}{|\langle\phi_0|\psi_0\rangle|^2} = 2N[f(-1) - \tfrac{1}{2}Q/N] \ ,$$

where we have included the term of order Q/N omitted in the computation of the entire spectrum. In the strongly coupled BCS theory

$$\sum_{\substack{\text{first grouping of}\\ \text{excited states}}} \frac{|\langle\phi_0|\psi_1\rangle|^2}{|\langle\phi_0|\psi_0\rangle|^2} = 2N - 1 \ . \tag{5.76}$$

In the GBCS model the ground state has a nonzero matrix element with all of the first excited states in which an excited pair has zero total momentum and the coherent background has zero total momentum (these are the excitations of the BCS case) and, in addition, there are matrix elements for which there are two excited "single" excitations of nonzero momentum against the coherent background of nonzero momentum such that the total momentum (two single excitations + coherent background) = 0. Presumably more than two excited "single" excitations lead to higher excited states. If we assume that these latter matrix elements are small compared to the first, we obtain

$$2N[f(-1) - \tfrac{1}{2}Q/N] \lesssim 2N - 1 \tag{5.77}$$

or

$$f(-1) \lesssim 1 + (Q-1)/2N \ , \tag{5.78}$$

which is consistent with (5.75).

VI. CONCLUSION

The following assumptions were made in arriving at our results: (i) restriction of the Hilbert space under consideration to the interaction region, (ii) replacement of the kinetic-energy operator by its expectation value ($T \to \langle T\rangle$), (iii) replacement of the most general two-body interaction by a spin-independent constant over the interaction region, (iv) extraction of the GBCS graphs from the totality of graphs generated by the strongly coupled Hamiltonian, and (v) approximation of the weight of subsets

of the GBCS graphs according to the number of cycles of which they are composed: the $f(\alpha)$ model.

We regard (i)–(iii) as simplifications of the full many-body problem which may change results in a quantitative way but are not likely to affect the qualitative results. It seems probable that a limit in which (i) is rigorous can be defined; (ii) certainly changes the numerical results and may alter the analytic properties of some of the interesting functions, but probably does not affect the qualitative nature of the results; and (iii) is relatively trivial and is made primarily for simplification. Altogether the system with the restrictions imposed by (i), (ii), and (iii) is of great complexity and retains most of the interesting properties of a many-fermion system; the results obtained can probably be generalized without these restrictions.

The approximation implied by (iv) is more serious. We regard this in the following way: The GBCS graphs are distinguished from the totality of graphs generated by the strongly coupled Hamiltonian by the fact that the vertices of which they are composed contain contributions when the momentum of the pairs being scattered approaches zero. In the limit that the pair momentum approaches zero, these are the only graphs that contribute; if one believes that the problem is dominated by the scattering of electron pairs of small (but not necessarily zero) total momentum, these are the graphs that dominate. Thus the GBCS graphs are a generalization of the usual BCS graphs in which one is not restricted to the exact $-\vec{k}\downarrow$, $\vec{k}\uparrow$ pairing.

The dominance of low-momentum pair scattering itself would be a consequence of the smallness of what we believe is the relevant parameter of the problem,

$$Q/N \sim (\delta/k_F)^2 ,$$

where δ/k_F is the ratio of the thickness of the interaction shell to the Fermi momentum. Of all the graphs generated by the full strongly coupled Hamiltonian, the ladder graphs are of the lowest order in this parameter: $(Q/N)^0$. However, by the arguments of Sec. II, it is clear that the ladder graphs by themselves will not suffice. We can then regard the graphs which constitute the GBCS system as a completion of the ladder graphs—a completion

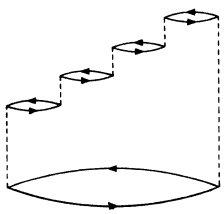

FIG. 27. A process which is not generated by the GBCS Hamiltonian.

which allows us to calculate the matrix elements of the U matrix in a conventional way, without the inclusion of exclusion-principle-violating processes, with errors of the order Q/N.

The approximations contained in (v) which lead to the $f(\alpha)$ model no doubt alter the results and can probably be improved in various ways, but we feel that this yields a fairly accurate estimate of the level structure.

Many of the graphs generated by the vertices omitted in the GBCS Hamiltonian will serve only to renormalize the various propagators and vertices. There will, however, always remain processes which are not included in the GBCS Hamiltonian such as those shown in Fig. 27 which will generate another branch of excitations. For a neutral Fermi gas it is known that these will result in collective modes where the lowest excitations are not separated from the ground state by any energy gap.

The graphs included in the GBCS system seem therefore to produce a qualitative account of the single-particle part of the spectrum of a many-fermion system subject to a weak attractive interaction. Although the ground state of the GBCS system is lower than that of the BCS system (consistent with the variational nature of the BCS ground-state wave function) and the higher excited states are spread about the BCS levels, it is striking that the energy gap between the ground state and the first excited states remains exactly as it is in the BCS theory. It therefore seems reasonable to conclude that the inclusion of the interaction between an electron $-\vec{k}\downarrow$ and the large number of electrons in the sphere surrounding $\vec{k}\uparrow$ does not destroy this most characteristic feature of the superconductor spectrum.

APPENDIX A: EVALUATION OF $S_n^{(1)}$ AND $S_n^{(2)}$

We have seen in Sec. III that a given graph can be decomposed uniquely into certain cycles. If all graphs in a given set of graphs can be decomposed into certain typical cycles, the number of graphs in this set can be found as the number of possible ways these typical cycles can be combined to form connected diagrams. Hence the counting problem becomes the problem of finding the typical cycles and their possible combinations. Using this approach we now find $S_n^{(1)}$ and $S_n^{(2)}$.

Evaluation of $S_n^{(1)}$. $S_n^{(1)}$ is the number of topological nonequivalent nth-order connected diagrams which are composed of $(n-1)$ cycles. If we write $v_1, v_2, v_3 \ldots v_{n-1}$ for the number of Gaudin decomposed vertices being connected in these $(n-1)$ cycles, we must have

$$v_1 + v_2 + v_3 \cdots + v_{n-1} = 2n , \tag{A1}$$

in such a way that

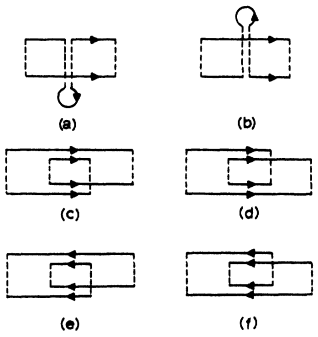

FIG. 28. Cycles connecting four vertices.

$$v_1 = v_2 = \cdots v_{n-2} = 2, \quad v_{n-1} = 4. \tag{A2}$$

From this we see that out of these cycles $(n-2)$ are elementary cycles which each connect two vertices, and one is a cycle connecting four vertices. The cycles in such a graph can therefore be characterized by a number series containing one 4 and $(n-2)$ 2's as below:

$$(4;\ 2,\ 2,\ \ldots\ 2)\ .$$

The cycles which connect four vertices, are shown in Fig. 28.

$S_n^{(1)}$ will be equal to the number of ways we can combine the cycles in Fig. 28 with the $(n-2)$ elementary cycles into diagrams. In order to simplify the counting problem we will exploit certain graphical symmetries. A BCS diagram represents a singlet interaction. A spin-up line will therefore never be connected to a spin-down line, and the diagram will as a result be divided into an upper and lower part. Hence for a given diagram, ladder diagrams excluded, there exists another topological nonequivalent diagram where the upper and lower parts are interchanged as compared to the first one. This is shown in Fig. 29. The only difference between the cycles from the two diagrams is that the upper and lower parts of the non-

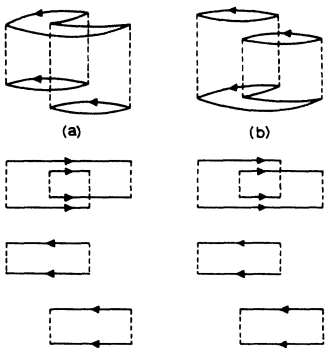

FIG. 29. Diagrams with upper and lower parts interchanged.

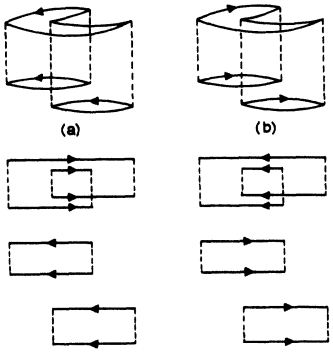

FIG. 30. Diagrams with opposite arrow direction.

elementary cycle are interchanged. Hence, in order to find $S_n^{(1)}$ we need only to consider combinations of parts (a), (c), and (e) in Fig. 28 and the $(n-2)$ elementary cycles, and then multiply the answer by 2.

In Fig. 30 we exhibit two diagrams of the same form, but with opposite arrow direction. These diagrams are topologically distinct. The only difference between diagrams (a) and (b) is that all the cycles in (b) have the opposite direction to the corresponding cycles in (a). Once again, it is sufficient to consider only half of such diagrams. However, not all graphs have another graph which is obtained by arrow reversal. This is the case for a graph which contains a cycle with a bubble. The reason, as mentioned before, is that the bubble can only exist in a cycle consisting of hole lines. $S_n^{(1)}$ will therefore be equal to the number of combinations of cycles (a) and (c), in Fig. 28, and the $(n-2)$ elementary cycles which give a connected diagram when the number of combinations with cycle (a) is multiplied by 2 and that with cycle (c) by 4.

As shown in Fig. 28 cycle (a) contains parts of three vertices. Since we have n vertices, there are altogether

$$\binom{n}{3}$$

different ways such a cycle can be placed among the vertices. In this cycle there can be no further connections to the vertex in the middle. Hence this vertex can be considered removed from the counting process. In order to have a connected graph we must require, $n = 3$ excluded, that the end vertices are not connected by an elementary cycle. We can therefore think of this unit [that is, the not yet connected Gaudin decomposed vertices left at the place cycle (a) occupied] as one vertex where lines go in and out. This means we have $(n-2)$ vertices which can be connected together ladderwise in $(n-3)!$ different ways. The total

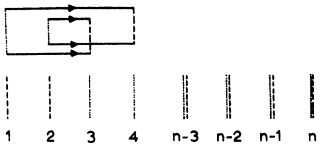

FIG. 31. Gaudin decomposed vertices to be linked together to a connected diagram.

number of combinations containing cycle (a) in Fig. 28 is therefore

$$2\binom{n}{3}(n-3)! \quad . \tag{A3}$$

Cycle (c) in Fig. 28 can be placed among the n vertices in

$$\binom{n}{4}$$

different ways. One arrangement is shown in Fig. 31. We let a dashed vertical line represent the Gaudin vertex part where lines come in, a dotted line where lines go out. At vertices 1, 2, 3, and 4 there are only single vertical lines left after we have placed the cycle (c) among these vertices. Starting, for example, at vertex n we can go out from that vertex into $(n-3)$ vertices. From one of these we can again go out into $(n-4)$ vertices, etc. If we, for the first time, come into either the vertex 1 or 2, let us say 2, we can go out from either vertex 3 or 4 into vertex 1 or any vertex where we have a double vertical line. This gives an additional factor 2 as compared to the case where we have $(n-2)$ vertices connected together ladderwise. Hence, the total number of ways of linking these vertices together is $2(n-3)!$. The total number of combinations containing cycle (c) in Fig. 28 is therefore

$$8\binom{n}{4}(n-3)! \quad , \tag{A4}$$

and finally

$$S_n^{(1)} = 2\binom{n}{3}(n-3)! + 8\binom{n}{4}(n-3)!$$

$$= 2\binom{n}{3}(n-2)! = \frac{n-2}{3}\,n! \tag{A5}$$

Evaluation of $S_n^{(2)}$. $S_n^{(2)}$ is the number of topological nonequivalent nth-order connected diagrams which are composed of $(n-2)$ cycles. As for $S_n^{(1)}$, we classify the cycles according to the number of Gaudin decomposed vertices they connect. From Eq. (A1) we see that the diagrams which are composed of $(n-2)$ cycles, to be counted here, must have one of the following two distributions of vertices:

I: $(6; 2, 2, 2, \ldots 2)$,

which contains $n-3$ elementary cycles of two vertices,

II: $(4, 4; 2, 2 \ldots 2)$,

which contains $n-4$ elementary cycles of two vertices. The sum of vertices is $2n$ as required. $S_n^{(2)}$ is now obtained in the same way as we found $S_n^{(1)}$; that is, as the total number of ways we can combine such cycles into connected diagrams. However, for two reasons, the calculation is now somewhat more complicated.

First, if we look at diagrams of the type I, they consist of one nonelementary cycle and $(n-3)$ elementary cycles. The number of such graphs are found in exactly the same way as for the case with $(n-1)$ cycles. The only difference is that there are many more cycles which connect six vertices than those connecting four, hence more possibilities.

The nonelementary cycles in group II are the same cycles as those shown in Fig. 28, but now there are two of them in each diagram. Just as in the calculation of $S_n^{(1)}$, we need here only to consider cycles (a) and (c) of Fig. 28 and their combinations. Since the relative positions of the nonelementary cycles turn out to be important, we study subgroups where these two cycles have 4, 3, 2, 1, or zero vertices in common. We then considered these combinations of the two cycles as one unit to be placed, as before, among the n vertices.

The combinatorial problem therefore falls into three parts. First, we must find how many different ways a certain unit can be placed among the n vertices. Second, we must calculate the number of ways the Gaudin decomposed vertices not being connected in this unit can be linked together ladderwise so as to form a connected diagram. Last, we have the somewhat more difficult problem of finding in how many topologically different ways we can form a given unit.

The first two parts are easily worked out. Suppose the unit in question covers j vertices; then such a unit can be placed among the n vertices in

$$\binom{n}{j}$$

ways. In Fig. 32 are shown typical examples of

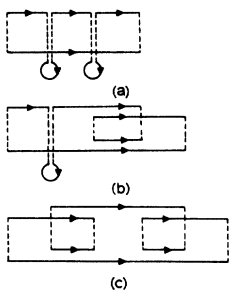

FIG. 32. Typical cycles connecting six Gaudin decomposed vertices.

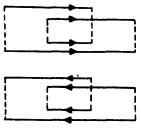

FIG. 33. A fourth-order diagram composed from two cycles, each connecting four vertices.

cycles connecting six Gaudin decomposed vertices. The unit in type-I graphs is seen to cover from four to six vertices. The unit in the type-II graphs, where the nonelementary cycles share at least one vertex, covers from four to seven vertices. The case with four vertices covered is exceptional since it only gives a connected diagram for $n=4$. This is shown in Fig. 33. Typical examples of combinations covering from five to seven vertices are shown in Fig. 34.

Finally, we have the possibility that the two nonelementary cycles have no vertex in common. This is shown in Fig. 35.

These combinations give the factors

$$\binom{n}{3}\binom{n-3}{3},\quad \binom{n}{3}\binom{n-3}{4},\quad \binom{n}{4}\binom{n-4}{4}\ . \tag{A6}$$

Since the two cycles in Figs. 35(a) and 35(c) are identical, some care must be taken in order to avoid double counting. We shall return to this point later.

The next part in the evaluation of $S_n^{(2)}$ is to find in how many different ways the Gaudin decomposed vertices, which are not connected by the nonelementary cycles, can be linked together by elementary cycles to form a connected diagram. This we do in exactly the same way as we treated the case shown in Fig. 31. We find that the cycles shown in Figs. 32(a)–32(c) can be linked together to a connected diagram by the elementary cycles in, respectively, the following number of ways:

$$(n-4)!,\quad 2(n-4)!,\quad 3(n-4)!\ . \tag{A7}$$

Using the same approach, we find for the type-II combinations of cycles shown in Fig. 34, where the two nonelementary cycles have 3, 2, and 1 vertices in common, that these cycles can be linked together in, respectively,

$$(n-5)!,\quad 2(n-5)!,\quad 3(n-5)! \tag{A8}$$

different ways.

Finally we have to consider the cases where the two nonelementary cycles have no vertices in common, that is the cases shown in Figs. 35(a)–35(c). Here special care must be taken not to count combinations which result in disconnected diagrams. We find the following number of different ways to link these cycles together to a connected diagram:

$$(n-5)!,\quad 2(n-5)!,\quad 4\times\tfrac{20}{24}(n-5)!\ . \tag{A9}$$

For $n=8$ there are 20 different ways of linking those Gaudin decomposed vertices, which are left after the cycles shown in Fig. 35(c) have been formed, together to a connected diagram. This verifies the last expression in (A9) for $n=8$.

We now consider the last part of the problem in evaluating $S_n^{(2)}$: finding all the topologically distinct ways of drawing a certain unit. As in the evaluation of $S_n^{(1)}$ we try to reduce the counting problem by exploiting the fact that interchanging upper and lower parts of a graph or reversing the arrows in a given graph gives a topologically different graph. The number of basic combinations are most easily obtained by simply drawing all the irreducible topological possibilities. The different units are treated in subgroups according to the number of vertices they cover. The details of this analysis will be published elsewhere; we here give the final result for $S_n^{(2)}$:

$$S_n^{(2)}=\left[4\binom{n}{4}+48\binom{n}{5}+96\binom{n}{6}\right](n-4)!+\left[84\binom{n}{5}+784\binom{n}{6}+1680\binom{n}{7}\right.$$
$$\left.+2\binom{n}{3}\binom{n-3}{3}+16\binom{n}{3}\binom{n-3}{4}+\frac{80}{3}\binom{n}{4}\binom{n-4}{4}\right](n-5)!+4\delta(n-4)\ . \tag{A10}$$

For $n=4$, 5, 6, and 7 this formula must be interpreted carefully. For $n=5$, for example, a term like

$$96\binom{n}{6}(n-4)!$$

does not contribute since this term comes from placing a cycle covering six vertices and we only have five vertices in a fifth-order graph. For $n\geq 8$ we find

$$S_n^{(2)}=n!\,(\tfrac{5}{108}n^3-\tfrac{23}{90}n^2+\tfrac{221}{540}n-\tfrac{8}{45})\ . \tag{A11}$$

APPENDIX B: ANALYSIS OF WEIGHT FACTORS FOR ALL GRAPHS WITH $\alpha=1$ AND 2 BY POLYGON METHOD; ASYMPTOTIC LIMITS

Graphs with $\alpha=1$. Graphs in this group are composed of one nonelementary cycle connecting four Gaudin decomposed vertices and $(n-2)$ elementary cycles. For $n>4$ the elementary cycles must be linked together in ladderlike chains. Summations over pair momentum $\vec{q}$ in such a chain can be replaced by a single elementary cycle; the effect of such ladderlike chains of elementary cycles

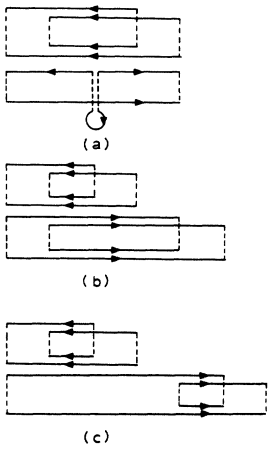

FIG. 34. Typical combinations of two cycles each connecting four vertices.

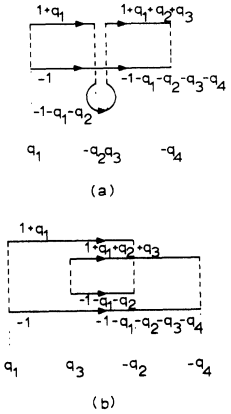

FIG. 36. Cycles giving four-point nonreduced polygons.

is just to establish identities between the pair momenta in the four-point polygon. It is therefore sufficient to look at a fourth-order graph. As explained in Appendix A the basic nonelementary cycles in this class can be Figs. 28(a) and 28(d). These two cycles are then labelled according to our conventions, see Fig. 36. They both give a four-point polygon as shown in Fig. 37(a). The elementary cycles can now be connected with the nonelementary cycles in two ways giving two sets of possible identies between the pair momenta,

$$\vec{q}_1 = -\vec{q}_2 , \quad \vec{q}_3 = -\vec{q}_4$$

or

$$\vec{q}_1 = -\vec{q}_4 , \quad \vec{q}_3 = -\vec{q}_2 .$$

We note that the last will always occur when the cycle contains a bubble. In both cases the four-point polygon is reduced to one of the three-point polygons shown in Fig. 37(b). All the three-point polygons (thus all graphs with $n-1$ cycles or $\alpha = 1$) have the same weight so that

$$N^{n-2} \sum_{\vec{q}_1 \vec{q}_2} N_2(\vec{q}_1 \vec{q}_2) = QN^n \left(\frac{Q}{N}\right) f[\alpha = 1] . \quad \text{(B1)}$$

Graphs with $\alpha = 2$. As in the evaluation of $S_n^{(2)}$, we treat this case in two parts according to the two possible distributions of vertices among the $(n-2)$ cycles. We first look at the case in which there are $(n-3)$ elementary cycles where the number of vertices has the distribution

$$(6; 2, 2, 2 \ldots 2) .$$

Here again the role of the elementary cycles will be to establish identities among the pair momenta in the six-point polygon coming from the cycle in which six Gaudin decomposed vertices are connected. In Fig. 38 such a cycle and its nonreduced polygon are shown. Since the elementary cycles will be linked to this cycle so as to form a connected diagram, they will establish identities between the pair momenta $\vec{q}_1$, $\vec{q}_3$, $\vec{q}_5$ and $-\vec{q}_2$, $-\vec{q}_4$, $-\vec{q}_6$. This is done in all possible ways, which for this case is six. The resulting possible identities among the pair momenta are as follows:

$$\begin{aligned}
&\text{(a)}\ \vec{q}_1 = -\vec{q}_2 , \quad \vec{q}_3 = -\vec{q}_4 , \quad \vec{q}_5 = -\vec{q}_6 ,\\
&\text{(b)}\ \vec{q}_1 = -\vec{q}_2 , \quad \vec{q}_3 = -\vec{q}_6 , \quad \vec{q}_5 = -\vec{q}_4 ,\\
&\text{(c)}\ \vec{q}_1 = -\vec{q}_4 , \quad \vec{q}_3 = -\vec{q}_2 , \quad \vec{q}_5 = -\vec{q}_6 ,\\
&\text{(d)}\ \vec{q}_1 = -\vec{q}_4 , \quad \vec{q}_3 = -\vec{q}_6 , \quad \vec{q}_5 = -\vec{q}_2 ,\\
&\text{(e)}\ \vec{q}_1 = -\vec{q}_6 , \quad \vec{q}_3 = -\vec{q}_2 , \quad \vec{q}_5 = -\vec{q}_4 ,\\
&\text{(f)}\ \vec{q}_1 = -\vec{q}_6 , \quad \vec{q}_3 = -\vec{q}_4 , \quad \vec{q}_5 = -\vec{q}_2 .
\end{aligned} \quad \text{(B2)}$$

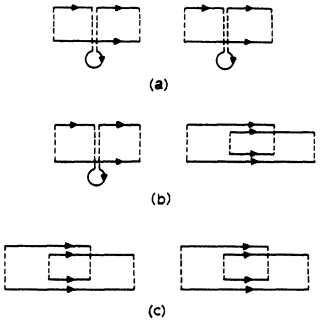

FIG. 35. Cycles each connecting four vertices but with no common vertex.

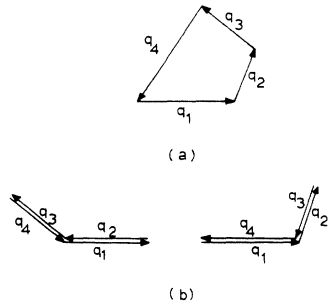

FIG. 37. Original polygon (a) and reduced polygons (b) for the cycles of Fig. 36.

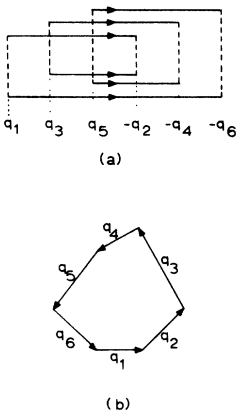

FIG. 38. Cycle connecting six vertices and its nonreduced polygon.

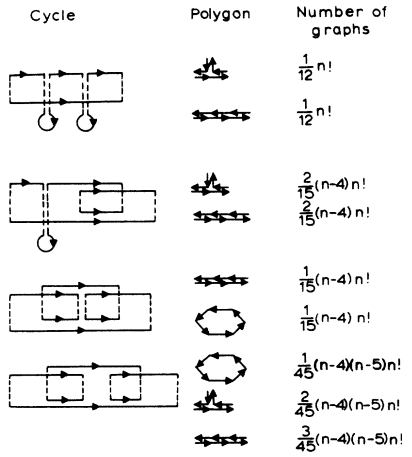

FIG. 40. Results of detailed analysis for graphs of the form (6; 2, 2, ...).

The corresponding reduced polygons are shown in Fig. 39. We see that polygon (a) = polygon (e) and polygon (b) = polygon (c) = polygon (f). The polygon (d) will in some situations give the same weight as (b), (c), or (f). In general, however, it may be different. We therefore have three types of reduced four-point polygons. The graphs with $\alpha = 2$ must now be examined in order to find how many graphs give polygon (a), (b), or (d).

We first look at the graphs containing a nonelementary cycle of the type shown in Fig. 32(a). In such a cycle the bubbles can be in four different positions, each topologically different. We first look at the case shown in Fig. 32(a). According to our labelling convention this part must give the identities

$$\vec{q}_1 = -\vec{q}_6, \quad \vec{q}_3 = -\vec{q}_2, \quad \vec{q}_5 = -\vec{q}_4 .$$

From (B2) it is seen this gives the polygon Fig. 39(e). If both bubbles are in the top position, we find the same polygon. However, if one bubble is in the up position, the other in the down position, we find the polygon Fig. 39(c). There is an equal number of graphs giving these two polygons. Since the total number of such graphs is known from Appendix A, we conclude that there are

$$2\binom{n}{4}(n-4)!$$

graphs giving, respectively, polygon Fig. 39(e) and polygon Fig. 39(c).

The case shown in Fig. 32(b) must satisfy one of the following set of identities:

$$\vec{q}_1 = -\vec{q}_4, \quad \vec{q}_3 = -\vec{q}_2, \quad \vec{q}_5 = -\vec{q}_6$$

or

$$\vec{q}_1 = -\vec{q}_6, \quad \vec{q}_3 = -\vec{q}_2, \quad \vec{q}_5 = -\vec{q}_4 .$$

These give an equal number of graphs with polygon Fig. 39(a) and polygon Fig. 39(b). However, the bubble can be in altogether eight different positions each giving a topologically different cycle. A similar inspection of the other seven possibilities gives the same result as for the case shown in Fig. 32(b). We therefore conclude there are an equal number of graphs of this type giving polygons (a) and (b). The result from a similar examination of all graphs in the subgroup characterized by the distribution (6; 2, 2, ... 2) is shown in Fig. 40.

We now consider the subgroup of graphs characterized by the distribution

$$(4, 4; 2, 2, \ldots 2) .$$

A typical example of this is shown in Fig. 41(a). Each of these cycles gives a nonreduced four-point polygon as in Fig. 37(a). In order to obtain the reduced polygons we must again connect these two cycles in all possible ways via elementary cycles. The role of the elementary cycles is, as before, to establish identities between the momenta $\vec{q}_1$, $\vec{q}_3$, $\vec{q}_5$, $\vec{q}_7$ and $-\vec{q}_2$, $-\vec{q}_4$, $-\vec{q}_6$, $-\vec{q}_8$. There are now 24 possible ways such connections can be made. However, not all need be considered; four con-

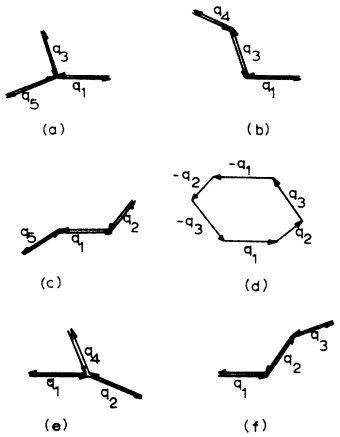

FIG. 39. The six reduced polygons.

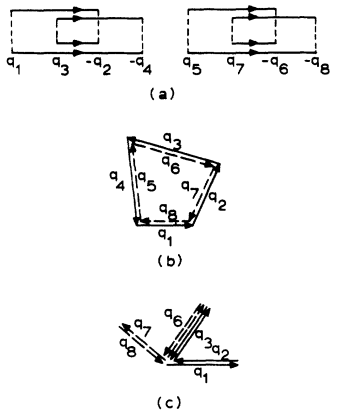

FIG. 41. Reduced polygons for the cycles (a).

nections give disconnected graphs. Thus there are 20 possible connections to be treated. The following lists the possible identities between the pair momenta:

(1) $\vec{q}_1 = -\vec{q}_2, \quad \vec{q}_3 = -\vec{q}_4, \quad \vec{q}_5 = -\vec{q}_6, \quad \vec{q}_7 = -\vec{q}_8,$

(2) $\vec{q}_1 = -\vec{q}_2, \quad \vec{q}_3 = -\vec{q}_4, \quad \vec{q}_5 = -\vec{q}_8, \quad \vec{q}_7 = -\vec{q}_6,$

(3) $\vec{q}_1 = -\vec{q}_2, \quad \vec{q}_3 = -\vec{q}_6, \quad \vec{q}_5 = -\vec{q}_4, \quad \vec{q}_7 = -\vec{q}_8,$

(4) $\vec{q}_1 = -\vec{q}_2, \quad \vec{q}_3 = -\vec{q}_6, \quad \vec{q}_5 = -\vec{q}_8, \quad \vec{q}_7 = -\vec{q}_4,$

(5) $\vec{q}_1 = -\vec{q}_2, \quad \vec{q}_3 = -\vec{q}_8, \quad \vec{q}_5 = -\vec{q}_4, \quad \vec{q}_7 = -\vec{q}_6,$

(6) $\vec{q}_1 = -\vec{q}_2, \quad \vec{q}_3 = -\vec{q}_8, \quad \vec{q}_5 = -\vec{q}_6, \quad \vec{q}_7 = -\vec{q}_4,$

(7) $\vec{q}_1 = -\vec{q}_4, \quad \vec{q}_3 = -\vec{q}_2, \quad \vec{q}_5 = -\vec{q}_6, \quad \vec{q}_7 = -\vec{q}_8,$

(8) $\vec{q}_1 = -\vec{q}_4, \quad \vec{q}_3 = -\vec{q}_2, \quad \vec{q}_5 = -\vec{q}_8, \quad \vec{q}_7 = -\vec{q}_6,$

(9) $\vec{q}_1 = -\vec{q}_4, \quad \vec{q}_3 = -\vec{q}_6, \quad \vec{q}_5 = -\vec{q}_2, \quad \vec{q}_7 = -\vec{q}_8,$

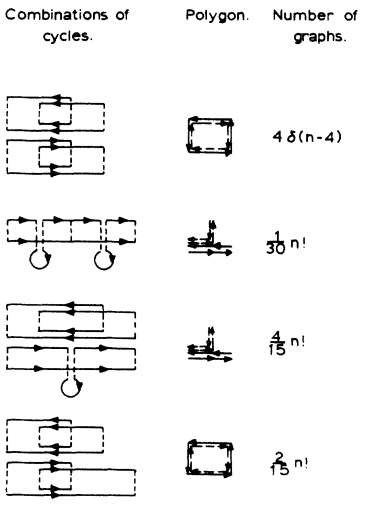

FIG. 42. Results of detailed analysis for graphs of the form (4, 4; 2, 2, ...).

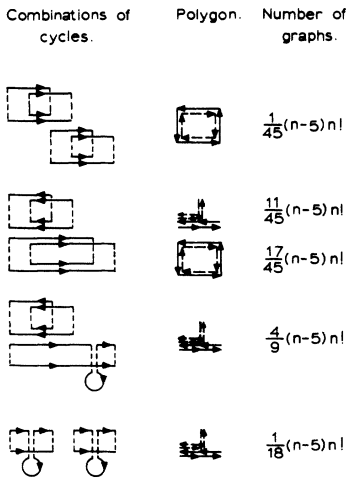

FIG. 43. Results of detailed analysis for graphs of the form (4, 4; 2, 2, ...).

(10) $\vec{q}_1 = -\vec{q}_4, \quad \vec{q}_3 = -\vec{q}_6, \quad \vec{q}_5 = -\vec{q}_8, \quad \vec{q}_7 = -\vec{q}_2,$

(11) $\vec{q}_1 = -\vec{q}_4, \quad \vec{q}_3 = -\vec{q}_8, \quad \vec{q}_5 = -\vec{q}_2, \quad \vec{q}_7 = -\vec{q}_6,$

(12) $\vec{q}_1 = -\vec{q}_4, \quad \vec{q}_3 = -\vec{q}_8, \quad \vec{q}_5 = -\vec{q}_6, \quad \vec{q}_7 = -\vec{q}_2,$

(13) $\vec{q}_1 = -\vec{q}_6, \quad \vec{q}_3 = -\vec{q}_2, \quad \vec{q}_5 = -\vec{q}_4, \quad \vec{q}_7 = -\vec{q}_8,$

(14) $\vec{q}_1 = -\vec{q}_6, \quad \vec{q}_3 = -\vec{q}_2, \quad \vec{q}_5 = -\vec{q}_8, \quad \vec{q}_7 = -\vec{q}_4,$

(15) $\vec{q}_1 = -\vec{q}_6, \quad \vec{q}_3 = -\vec{q}_4, \quad \vec{q}_5 = -\vec{q}_2, \quad \vec{q}_7 = -\vec{q}_8,$

(16) $\vec{q}_1 = -\vec{q}_6, \quad \vec{q}_3 = -\vec{q}_4, \quad \vec{q}_5 = -\vec{q}_8, \quad \vec{q}_7 = -\vec{q}_2,$

(17) $\vec{q}_1 = -\vec{q}_6, \quad \vec{q}_3 = -\vec{q}_8, \quad \vec{q}_5 = -\vec{q}_2, \quad \vec{q}_7 = -\vec{q}_4,$

(18) $\vec{q}_1 = -\vec{q}_6, \quad \vec{q}_3 = -\vec{q}_8, \quad \vec{q}_5 = -\vec{q}_4, \quad \vec{q}_7 = -\vec{q}_2,$

(19) $\vec{q}_1 = -\vec{q}_8, \quad \vec{q}_3 = -\vec{q}_2, \quad \vec{q}_5 = -\vec{q}_4, \quad \vec{q}_7 = -\vec{q}_6,$

(20) $\vec{q}_1 = -\vec{q}_8, \quad \vec{q}_3 = -\vec{q}_2, \quad \vec{q}_5 = -\vec{q}_6, \quad \vec{q}_7 = -\vec{q}_4,$

(21) $\vec{q}_1 = -\vec{q}_8, \quad \vec{q}_3 = -\vec{q}_4, \quad \vec{q}_5 = -\vec{q}_2, \quad \vec{q}_7 = -\vec{q}_6,$

(22) $\vec{q}_1 = -\vec{q}_8, \quad \vec{q}_3 = -\vec{q}_4, \quad \vec{q}_5 = -\vec{q}_6, \quad \vec{q}_7 = -\vec{q}_2,$

(23) $\vec{q}_1 = -\vec{q}_8, \quad \vec{q}_3 = -\vec{q}_6, \quad \vec{q}_5 = -\vec{q}_2, \quad \vec{q}_7 = -\vec{q}_4,$

(24) $\vec{q}_1 = -\vec{q}_8, \quad \vec{q}_3 = -\vec{q}_6, \quad \vec{q}_5 = -\vec{q}_4, \quad \vec{q}_7 = -\vec{q}_2.$

(B3)

We see that the identities (1), (2), (7), and (8) correspond to disconnected diagrams. They are therefore excluded. An examination of the reduced polygons from the other 20 possibilities reveals that there are two types. They are shown in Figs. 41(b) and 41(c). It should be noted that the polygon shown in Fig. 41(c) represents a different sum over phase space than the polygon shown in Fig. 39(a). In Fig. 39(a) all the pair momenta come from one cycle; in Fig. 41(c) the pair momenta come from two cycles but have one momentum in common. Thus the weight contributed by Fig.

41(c) is the product of the weights of two three-point polygons with one momentum in common. We find that the polygons resulting from (17), (18), (23), and (24) are of the type shown in Fig. 41(b); all the other possibilities give the polygon of Fig. 41(c).

In exactly the same manner as for the graphs characterized by (6; 2, 2, ... 2), we now determine how many graphs give either type of polygon. The results are shown in Figs. 42–44.

We can summarize these results as follows. All graphs with $n-1$ cycles have the same weight given by (B1),

$$N^{n-2}\sum_{\vec{q}_1\vec{q}_2} N_2(\vec{q}_1\,\vec{q}_2) = QN^n\left(\frac{Q}{N}\right) f[\alpha=1]\ .$$

We can therefore identify $f[\alpha=1]$ with $f(\alpha=1)$ of (5.2),

$$f(1)=f[\alpha=1]\ . \tag{B4}$$

Thus the total contribution from the sum over all connected graphs with $n-1$ cycles ($\alpha=1$) is

$$S_n^{(1)}(-1)QN^n(Q/N)f(1). \tag{B5}$$

The phase-space sums associated with the various reduced polygons that are generated by the graphs with $\alpha=2$ can be written in a manner similar to (B1) as

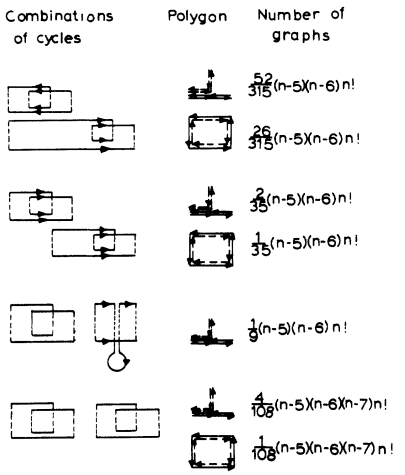

FIG. 44. Results of detailed analysis for graphs of the form (4, 4; 2, 2, ...).

$$QN^n(Q/N)^2 f[\hat{g}_{\alpha=2}]\ . \tag{B6}$$

The factors $f_1[\alpha=2]$, $f_2[\alpha=2]$, $f_3[\alpha=2]$, $f_4[\alpha=2]$, and $f_5[\alpha=2]$ come from the polygons (a), (b), and (d) of Fig. 39 and (b) and (c) of Fig. 41; the total contribution from graphs with $\alpha=2$ now can be written

$$\begin{aligned}QN^n(Q/N)^2 n!\{&f_1[\alpha=2][\tfrac{1}{12}+\tfrac{2}{15}(n-4)+\tfrac{2}{45}(n-4)(n-5)]+f_2[\alpha=2][\tfrac{1}{12}+\tfrac{2}{15}(n-4)+\tfrac{1}{15}(n-4)+\tfrac{3}{45}(n-4)(n-5)]\\&+f_3[\alpha=2][\tfrac{1}{15}(n-4)+\tfrac{1}{45}(n-4)(n-5)]+f_4[\alpha=2][4\delta(n-4)+\tfrac{2}{15}+\tfrac{1}{45}(n-5)+\tfrac{17}{45}(n-5)\\&+\tfrac{26}{315}(n-5)(n-6)+\tfrac{1}{35}(n-5)(n-6)+\tfrac{1}{108}(n-5)(n-6)(n-7)]\\&+f_5[\alpha=2][\tfrac{1}{30}+\tfrac{4}{15}+\tfrac{11}{45}(n-5)+\tfrac{4}{9}(n-5)+\tfrac{1}{18}(n-5)+\tfrac{52}{315}(n-5)(n-6)+\tfrac{2}{35}(n-5)(n-6)\\&+\tfrac{1}{9}(n-5)(n-6)+\tfrac{4}{108}(n-5)(n-6)(n-7)]\}\ .\end{aligned} \tag{B7}$$

In the limit that $n\to\infty$, the term in brackets is dominated by

$$\lim_{n\to\infty}\{\cdots\}\to\frac{n^3}{108}f_4[\alpha=2]+\frac{4n^3}{108}f_5[\alpha=2] = \frac{n^3}{108}(f_4[\alpha=2]+4f_5[\alpha=2])\ . \tag{B8}$$

And in this same limit $S_n^{(2)}$ becomes

$$\lim_{n\to\infty} S_n^{(2)} = n!\frac{5n^3}{108}\ . \tag{B9}$$

Thus when $n\to\infty$ we can write the sum over all connected graphs with $n-2$ cycles ($\alpha=2$) as

$$S_n^{(2)}(-1)^2QN^n(Q/N)^2f(2), \tag{B10}$$

where

$$f(2)=\tfrac{1}{5}(f_4[\alpha=2]+4f_5[\alpha=2])\ . \tag{B11}$$

Because the addition of ladder linkages does not alter the polygon structure, the sum over connected graphs with $n-\alpha$ cycles for values of α larger than 2 will in a similar manner be dominated as $n\to\infty$ by some specific combination of polygon functions in such a way that the contribution can be written

$$S_n^{(\alpha)}(-1)^\alpha QN^n(Q/N)^\alpha f(\alpha). \tag{B12}$$

This is the basis of the $f(\alpha)$ model analyzed in Sec. V.

*Work supported in part by the Advanced Research Projects Agency, the National Science Foundation, and the U. S. Atomic Energy Commission.

[1]Y. Wada, F. Takano, and N. Fukuda, Progr. Theoret.

Phys. (Kyoto) 19, 597 (1958).
[2]N. M. Hugenholtz and L. Van Hove, Physica 24, 363 (1958).
[3]P. W. Anderson, Phys. Rev. 112, 1900 (1958).
[4]D. J. Thouless, Phys. Rev. 117, 1256 (1960).
[5]L. N Cooper, Phys. Rev. 122, 1021 (1961).
[6]B. Stŏlan and L. N Cooper, Phys. Rev. 143, 209 (1966).
[7]N. M. Hugenholtz, Physica 23, 481 (1957); in *The Many-Body Problem*, edited by C. Dewitt and P. Nozières (Wiley, New York, 1959), p. 1.
[8]L. Van Hove, Physica 21, 901 (1955); 22, 343 (1956).
[9]G. C. Wick, Phys. Rev. 80, 268 (1950).
[10]E. C. Titchmarch, *The Theory of Functions*, 2nd ed. (Oxford U. P., Oxford, England, 1939), p. 250.
[11]J. Goldstone, Proc. Roy. Soc. (London) A239, 267 (1957).
[12]K. Fukushima and N. Fukuda, Progr. Theoret. Phys. (Kyoto) 28, 809 (1962).
[13]H. P. Kelly, Phys. Rev. 131, 684 (1963).
[14]M. Gaudin, Nucl. Phys. 20, 513 (1960).

PHYSICAL REVIEW B VOLUME 4, NUMBER 3 1 AUGUST 1971

Spin-Orbit Coupling and Nuclear Magnetic Resonance in Superconducting Metals*

W. A. Hines† and W. D. Knight
Department of Physics, University of California, Berkeley, California 94720
(Received May 14 1970)

In this work, the effect of spin-orbit coupling (through spin-reversing scattering) on the paramagnetic spin susceptibility of conduction electrons in a superconductor has been studied. This was accomplished by investigating the nuclear magnetic resonance of two groups of (type-I) superconducting samples. In the first group of samples, consisting of different-sized samples of pure lead, the residual NMR shift in the limit of zero temperature was found to vary with particle size, as is true for pure tin. The results are consistent with the existence of a larger spin-orbit interaction in lead. The second group of samples, containing various concentrations of In, Sb, Pb, and Bi impurities, exhibited residual NMR shifts which were consistent with the spin-orbit interactions characteristic of the respective impurities. Taken together, the NMR results are consistent with the microscopic theory of superconductivity, including the effects of spin-orbit interactions.

I. INTRODUCTION

In the 13 years that have passed since the development of the Bardeen, Cooper, and Schrieffer (BCS) theory,[1] most of the properties of superconductors have been explained. Using the BCS description, Yosida[2] calculated the conduction-electron paramagnetic spin susceptibility as a function of temperature for a superconductor, and as a result of the pairing of electronic spins, he predicted a vanishing susceptibility at $T = 0\,^{\circ}\mathrm{K}$. The electronic spin susceptibility may be investigated directly by measuring the shift of the nuclear magnetic resonance. For simple metals, the NMR shift has been attributed to the paramagnetism of the conduction-electron spins, together with their contact hyperfine interaction with the nucleus.[3] However, NMR experiments on various superconductors have shown a nonvanishing shift as the temperature is extrapolated to zero, in apparent disagreement with the theory.[4-6] Two general ideas have been proposed to explain the residual NMR shift in superconductors: (i) In a superconductor, the paramagnetic spin susceptibility (temperature dependent) is modified by spin-reversing scattering due either to the boundaries of the small specimens or to the presence of impurities,[7-9] and (ii) there exist other contributions to the shift which are temperature independent in the superconducting state.[10,11] (It must be remembered that because of the Meissner effect, NMR experiments in type-I superconductors have required samples such that at least one dimension is the order of a few hundred angstroms.) Recent work by Wright[12,13] on tin particles, in which the electronic mean free path was limited by varying the particle size, supports the spin-reversing scattering theory. He found that the residual shift was a function of the particle size and that the data fit the spin-reversing scattering theory best by assuming that any other contributions (temperature independent in the superconducting state) were unimportant. However, because only the electronic mean free path is varied, Wright's experiments alone do not demonstrate conclusively the effect of the spin-orbit coupling. It is the purpose of the present work to illustrate the effect of the spin-orbit coupling strength on the spin-reversing scattering and hence the electronic spin susceptibility. This has been done in two ways by performing two series of experiments. In